MICROMOTION AND SCARRING DO NOT CONTRIBUTE TO FAILURE OF REGENERATIVE PERIPHERAL NEURAL INTERFACING

by

NIVEDITA KHOBRAGADE

Presented to the Faculty of the Graduate School of

The University of Texas at Arlington in Partial Fulfillment

of the Requirements

for the Degree of

MASTER OF SCIENCE IN BIOMEDICAL ENGINEERING

THE UNIVERSITY OF TEXAS AT ARLINGTON

December 2011

ACKNOWLEDGEMENTS

I would like to first and foremost thank my father, Dr. Yadneshwar Khobragade and my mother, Dr. Sujata Khobragade, for their unvarying support and encouragement for my work, for trusting my decisions and for being my pillars of strength.

I am extremely grateful to my mentor, Dr. Mario Romero-Ortega, for giving me the opportunity to work in his laboratory and for helping me in fulfilling my desire of pursuing research in the field of Neuroengineering. I want to thank him for his inspiration and guidance throughout the course of my study and for honing my skills as a researcher. His innovative ideas and invaluable feedback always proved to be beneficial for my project.

I want to convey my sincere gratitude to Dr. Young-Tae Kim and Dr. George Alexandrakis for agreeing to be a part of my committee. I also want to thank them for helping me at different points of time during my Masters degree.

Lastly, I extend my thanks to all my colleagues and friends for their valuable advice, suggestions, encouragement and timely help.

December 6, 2011

ABSTRACT

MICROMOTION AND SCARRING DOES NOT CONTRIBUTE TO FAILURE OF REGENERATIVE PERIPHERAL NEURAL INTERFACING

Nivedita Khobragade, M.S.

The University of Texas at Arlington, 2011

Supervising Professor: Mario Romero-Ortega, PhD

Neuroprosthetics facilitate amputees with motor function restoration by interfacing nervous system with artificial limb and enabling control of the prosthetic device by volitional thought. Though such neurointerfacing provides dexterity nearly mimicking natural limb agility, the clinical viability of such prosthetics is limited by the lack of long-term reliability. In central nervous system, these implants fail due to foreign body reaction and glial scar formation around the implant. The cause of decrease in active sites of interfacing in peripheral nervous system, which is less invasive than central nervous system implantation, has not been established. Recently an open architecture, regenerative peripheral neural interface was developed which successfully records in amputated nerves as early as 7 days. A decline in the number of active electrodes is observed similar to other neural interfaces. To elucidate the cause of this decay, the tissue response was evaluated over chronic implantation of Regenerative Multi-electrode Interface (REMI) into the sciatic nerve of adult rats. Floating multi-electrode arrays comprising 18 Pt/Ir electrodes, placed in collagen-filled Polyurethane tubes, were implanted in eighteen female adult Lewis rats by suturing the stumps of transected sciatic nerve to the tube. Control animals were

twelve female adult Lewis rats which were implanted with collagen-filled Polyurethane conduits lacking FMAs by similar procedure following sciatic nerve transection. Electrophysiological recordings were carried out weekly using Omniplex data acquisition system (Plexon Inc. USA). Progressive decrease in the number of functional electrodes was observed after 21 days of implantation. The REMI-implanted sciatic nerve and the L4-L5 DRGs were harvested after 15, 30 and 60 days post-implantation (n=6 for each group). Reactive macrophages visualized by immunofluorescence of ED1 labeling, showed a significant decrease in the scar area after 60 days of implantation compared to 15-day post-surgery. Macrophage cell density did not increase from 15-day to 60-day post-implantation indicating that the scar area did not compact with time. Electrophysiological recordings were obtained at 15 days when inflammatory response had already encapsulated the electrode site suggesting that macrophage scar does not play a role in failure in recording capability of electrodes. Transcription factors ATF3 Activating Transcription Factor-3 and c-Jun, which are upregulated during nerve injury, were also assessed to determine if the electrodes were causing neuronal damage due to micromotion. ATF3 expression levels in REMI implanted animals had significantly reduced after 60 days of sciatic nerve transection compared to that after 15 days and the levels were not significantly different than control animals. cJun levels were significantly increased 60-days post-implantation compared to that at 15-days and were similar to cJun expression in control animals. This provides evidence that REMI implants form a stable interface with the regenerated nerve and are not affected by micromotion. Due to low susceptibility to micromotion, REMI interfacing does not aggravate inflammatory response or cause nerve damage at interface with chronic implantation.

TABLE OF CONTENTS

LIST OF ILLUSTRATIONS

LIST OF TABLES

CHAPTER 1

INTRODUCTION

1.1 Motivation

Over 2 million people have suffered limb loss in the United States, the number of amputees increases by approximately 185,000 annually (Darnall et al. 2005) and this figure is estimated to rise to 3.6 million by the year 2050 (Ziegler-Graham et al. 2008). Limb loss is a life-altering event that adversely impacts the physical, social, vocational and financial aspects of amputees (Dillingham et al. 2002). Disabled amputees can be fitted with artificial limbs to partially recover some function. However, control of such prosthetic devices is unnatural and depends mostly on myoelectric signal. To achieve natural control and feel, brain-machine interfaces and peripheral interfaces have been developed, and while they have proven feasible, they fail to serve reliably as nerve signals fail to be recorded overtime. Therefore, it is essential to elucidate the cause of failure of these interfaces to provide methods for natural long-term use of robotic limbs.

1.1.1 Etiology of limb loss

The most prevalent causes of limb loss are vascular diseases and trauma. In 2005, 54% of limb loss cases were due to vascular diseases, and 66% of them were diagnosed with comorbid diabetes. Trauma accounted for 44% cases of limb loss and the remaining 2% were the result of malignancy of bone or joint (Ziegler-Graham et al. 2008). Amputations secondary to vascular conditions in peripheral arterial diseases and diabetes are due to arterial damage. Atherosclerosis or the occlusion of the peripheral blood vessels causes ischemia leading to extensive tissue death (Garcia 2006, Mautner et al. 1992). Approximately 83% of non-traumatic lower-limb amputations are associated with diabetes mellitus-related complications (Fitzgerald et al. 2009). In diabetic patients, foot ulcers and infections that result from peripheral neuropathy

can also eventually lead to amputation (Reiber et al. 1999).Trauma-related limb loss may be due to accident-related or war-related injuries. Injuries due to casualties like motor vehicle collision, industrial accidents or environmental accidents can result into amputation if the damaged limb cannot be preserved. Combat-related injuries resulting in limb loss contribute to 7.4% of the major limb injuries. The wars in Iraq and Afghanistan - Operation Iraqi Freedom and Operation Enduring Freedom, respectively, have resulted in more than 1100 cases of limb amputations among the US troops (Kirk et al. 2011).From these, 69% comprise upper-limb amputations(Behrend et al. 2011). Congenital defects are also a source of limb deficiency and 10% of those born with congenital anomalies suffer from upper extremity differences (Chung 2011). Limb amputations are classified based on the level of amputation as either minor or major limb amputation (Figure1.1) (Dillingham et al. 1998).

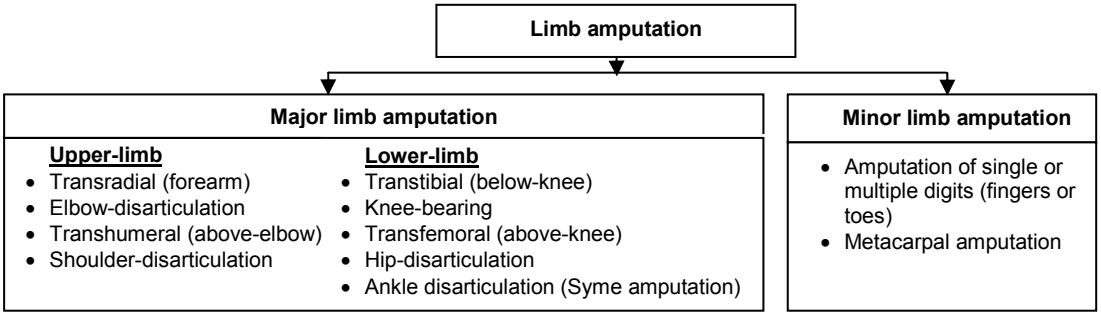

Figure 1.1 Types of major and minor limb amputations

Compromise in the quality of life depends on the level of amputation with the upper-limb amputees being more affected than those suffering with lower-limb amputation (Behrend et al. 2011). Development of operable upper-limb prosthetic devices is challenging due to the complex functional anatomy of hand. Lower-limb prosthesis functions include enabling the amputee to stand and walk whereas artificial arm functions demands a diverse set of tasks which vary from delicate to strong in nature.

1.2 Artificial Prostheses for Upper-limb

The use of prosthetic limbs dates back to fifteenth century BC, during the times of ancient Egyptians, where prostheses made of wood and leather provided cosmetic appearance and basic restoration of function such as mobility in case of lower-limb prosthesis. The materials used in artificial limbs like aluminum and steel have been replaced over the years with materials that are durable and light-weight such as plastic and silicone (Thurston 2007). Upper prosthetics require the use of a socket which assists in fitting the prosthetic limb to the arm stump, and supports the hand "terminal" prosthesis which allows the user to perform various tasks.

1.2.1 Terminal devices

Terminal devices such as hooks or prosthetic hands and are classified as passive or prehensile devices. While passive devices serve as non-functional components for cosmetic appearance or for static grasp, prehensile devices are terminal devices consisting of moving parts that allow the user to perform tasks such as grasping or manipulating objects [Figure 1.3 (A)].

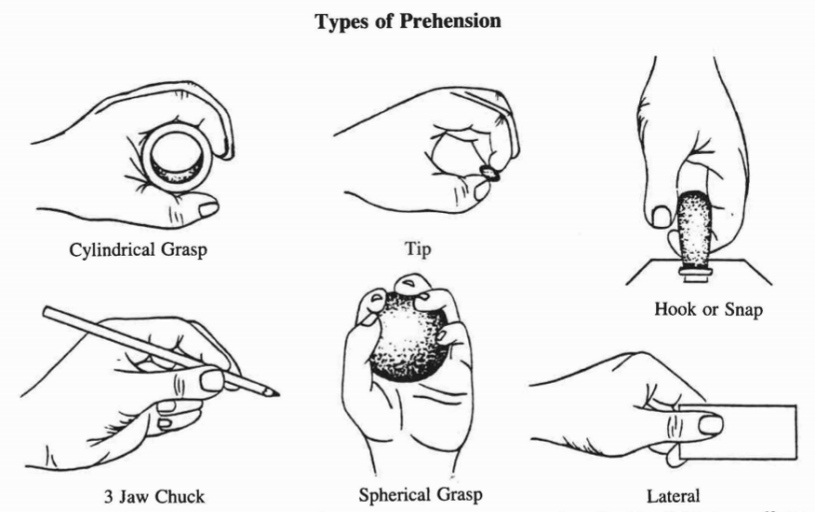

Figure 1.2 Types of Prehensile grasps (Billock 1986)

Mechanical terminal devices like hooks [Figure 1.3 (B)] and hands [Figure 1.3 (C)] were controlled manually prior to 1960s. Mechanical hooks provide 8-10 lbs of prehensile grasp and

are lighter than mechanical hands, and while much progress has been made on mechanical devices, the users are unable to actuate the same number of degrees of freedom compared to those by the human hand (i.e., 22; Soechting and Flanders 1996) or most recent multi-articulated electric arms. The electric hands, introduced clinically in 1960s, can provide 20-24 lbs of finger prehension and can allow “3 jaw chuck” type prehension. Despite the advantages, electric hands are not as popular as the mechanical devices due to its slow response time (Billock 1986). Recent development in terminal devices has made available articulated hands with higher degrees of freedom [Figure 1.3 (D)].

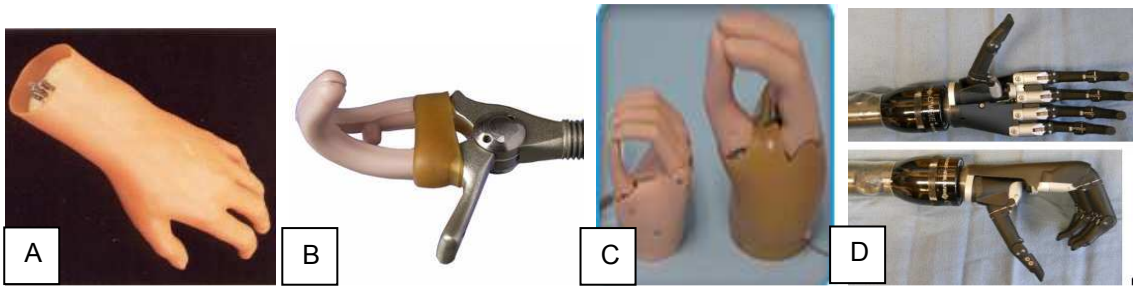

Figure 1.3 Types of terminal devices: (A) Passive hand (Health Related Products, Greenwood, SC), (B) Hooks (OttoBock, Germany), (C) Mechanical hand (Orthologix, Trevose, PA), (D) Multi-articulated hand (iLimb, Touch Bionics, Hilliard, OH)

1.2.2 Body-powered Prosthetics

Body-powered prostheses [Figure 1.4 (A) and (B)] were developed nearly a century ago. These cable-control systems can provide some functionality by enabling a mechanical hook or a terminal device to grasp or perform similar functions. The terminal device can be activated by harnessing the forces generated using flexion-abduction movements (Billock 1986).

Such prostheses cannot assist amputees with high-level amputations wherein operating the body-powered devices is not possible. These devices can only provide limited extent of movement and prehensile strength. Large amount of energy is required for the gross body movements, which are needed to perform the grasping function (Behrend et al. 2011).

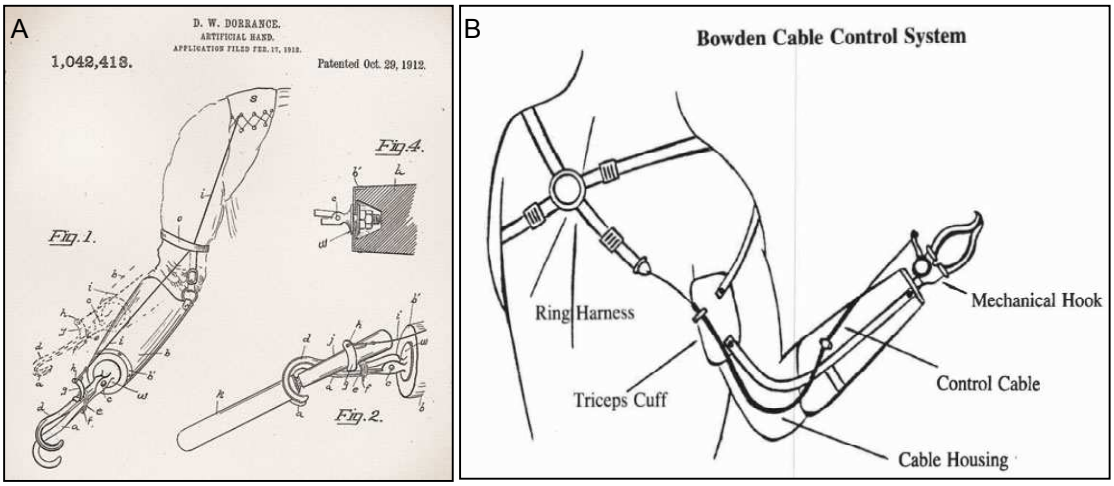

Figure 1.4 (A) & (B) (Billock 1986) Illustrations of typical body-powered cable-controlled prosthesis actuated by "gross" body movements

1.2.3 Myoelectric controlled systems

These devices allow control of an electromechanical terminal device by myoelectric signals [Figure 1.5 (A) & (B)]. The Electromyogenic (EMG) signals are measured by surface electrodes, amplified and converted to mechanical signals using actuators (Jacobsen et al. 1982). Such systems require considerably less energy and provide more comfort as compared to the body-powered prostheses (Billock 1986, Millstein et al. 1986).

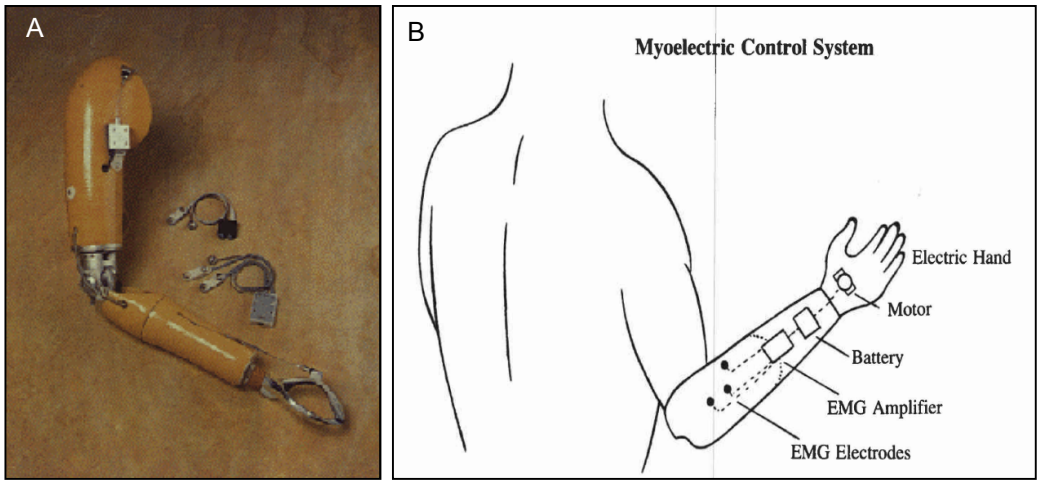

Figure 1.5 (A) & (B) (Billock 1986) Myoelectric externally-powered prosthesis

However, EMG signals, recorded at the skin surface, have high response time, thus require the patient to learn non-natural control strategies (Micera et al. 2010). To apply this technique, it is essential that the limb of the amputee has sufficient remnant muscle and nerve fibers. Myoelectric devices need to be externally powered, are heavy and require maintenance. These systems cannot provide a proprioceptive feedback, have limitations with prehension strength and allow only single function control at a time (Behrend et al. 2011).

1.2.4 Targeted reinnervation

Targeted muscle reinnervation (TMR), a method developed by Dr. Todd Kuiken, involves surgical remapping of nerves of the amputated limbs to a denervated spare muscle for enabling control of a prosthetic device. For example, in case of shoulder disarticulation, nerves formerly innervating the brachial plexus are redirected to the pectoral muscles [Figure 1.6 (A)]. The EMG signals from the reinnervated pectoral muscles can then drive a mechatronic arm voluntarily and can permit performance of multiple functions simultaneously [(Figure 1.6 (B)].

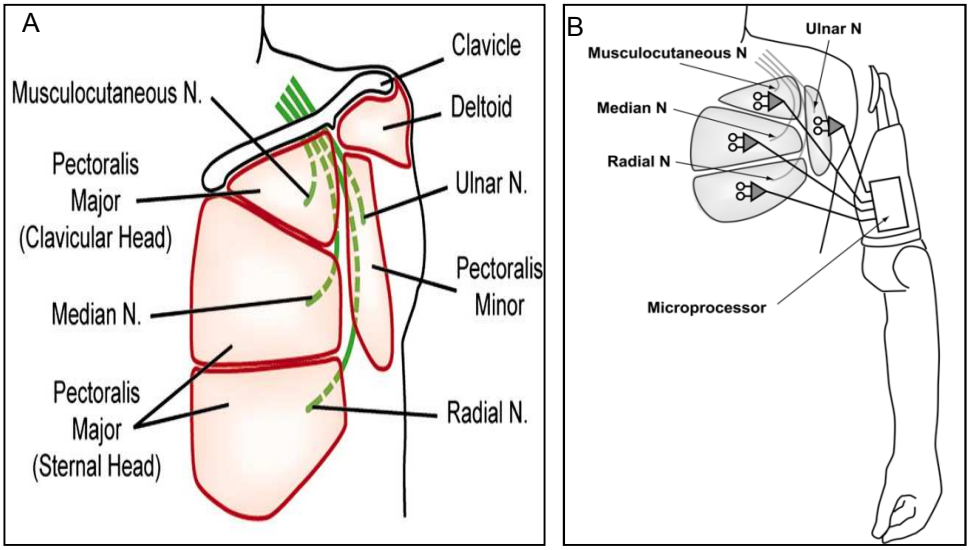

Figure 1.6 Targeted reinnervation: (A) Pectoralis major reinnervation by four major arm nerves (Kuiken et al. 2007(i)), (B) Electromyograph electrode placement for driving a programmed prosthetic arm (Stubblefield et al. 2009)

This procedure can be used even in case of higher level amputations such as shoulder disarticulation when compared to myoelectric-control prostheses which can be implemented

only in below-elbow or transradial amputations. The prosthesis user can also regain sensory feedback with targeted sensory reinnervation where the skin overlying the targeted muscle is denervated and reinnervated with the afferent nerve fibers of the amputated limb. Sensors in the artificial limb can measure parameters like pressure, texture, temperature and enable actuators to apply equivalent stimulus to the reinnervated skin (Kuiken 2006, Kuiken 2007(ii)). This technique is less invasive than other neural implants but leads to function-loss of the targeted muscle such as adduction of humerus by pectoralis major muscles. It involves certain risks such as phantom limb pain, neuromas and surgery failures. Repetitive recruitment of the reinnervated muscle fibers may result in muscle fatigue (Stuffblefield et al. 2009). Since the technique for prosthesis control is based on recording myoelectric signals, translation of the neural signals to motor functions necessitates complex algorithm and signal processing. Targeted muscle reinnervation prostheses, similar to myoelectric-based artificial limb, lack proprioceptive information and rely on visual and tactile feedback for control.

1.2.5 Electroencephalogram-based Prosthetic Control

Electroencephalogram is recorded for interpreting voluntary intentions of motion by measuring the electrical activity from large populations of motor cortical neurons using surface electrodes placed over the scalp. A decrease in the power of Mu waves with the frequency band of 8-12 Hz and Beta waves (18-25 Hz) is observed during motion. Prosthesis can be manipulated by modulating the amplitudes of these rhythms (Schwartz et al. 2006). Though the advantage of the method is its non-invasiveness, the major limitation of EEG-based systems is that the activity is recorded from the scalp, i.e. 2-3 cm away from the cortical surface. Due to the low spatial frequency, localized recording from the different areas of the motor cortex is not possible. Electrocorticogram (ECoG) uses non-penetrating electrodes which record from the surface of the cortex. This technique, though more invasive than EEG, improves the spatial and the temporal resolution and can be utilized to better control an artificial limb by modulating the high frequency gamma rhythms (Lebedev and Nicolelis 2006).

1.2.6 Micro-electrode arrays

Multiple micro-electrodes [Figure 1.7] can be implanted in the Central or the Peripheral nervous system to record the neural activity and extract the useful information for control of a prosthetic device (Warwick et al. 2003, Schulman 2009, and Serruya et al. 2002). The electrical activity comprises different frequency components - Single-unit activity (SUA)/ Multi-unit activity (MUA) (300-6000 Hz) or Local Field Potentials (8-200 Hz) (Mattia et al. 2010, Rees et al. 2002, and Andersen et al. 2004). Single Unit spike (SUS) is the activity of a single neuron which can be measured if the tip is sufficiently small (3-5 μm) and is close to the neuron. The ability to record distinguishable SUS also depends on the impedance and the shape of the microelectrode. The micro-electrodes provide high spatial resolution (100 μm) and high temporal resolution (50-100 Hz); thereby allowing dexterous control of the artificial limb.

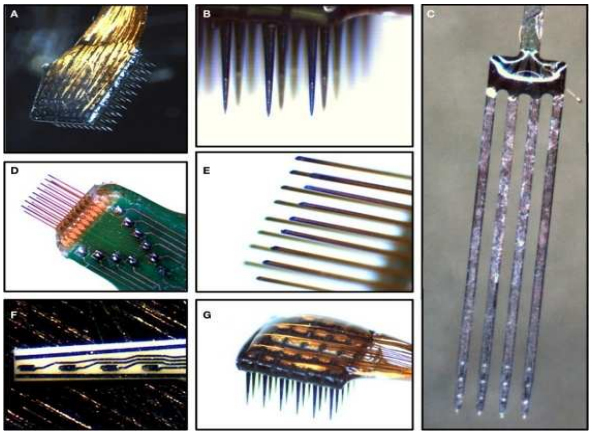

Figure 1.7 Different types of multielectrode arrays (Rothschild 2010)

Multi-unit recording is the activity measured from several neurons near-by the electrode. Local Field Potentials, which is a measure of the net activity of local population of neurons, can be recorded from micro-electrode arrays (MEAs). This lower frequency component (<200 Hz) is less affected by the location of the electrode but does not provide the same level of control as single unit spikes (Schwartz et al. 2006, Lebedev and Nicolelis 2006).

Although the multi-electrode arrays (MEA) are capable of providing intuitive control, dexterity of prosthetic limb and sensory feedback, the implantation of such interfaces is

extremely invasive (Lebedev and Nicolelis 2006). The electrodes cause severe foreign body-tissue response at the site of implantation prohibiting chronic use of such arrays.

1.2.7 Implantation site-based classification of multi-electrode interfacing

The multi-electrodes are implanted to directly contact the nervous system for sensing and deciphering the neural signals to drive a robotic prosthesis. The neural interfacing can be classified based on the site of implantation as Central Nervous System (CNS) neural interface or Peripheral Nervous System (PNS) neural interface. In CNS interfaces or Brain Machine Interfaces (BMI), the multi-electrodes are implanted in the primary motor cortex to record from the cortical neurons and decode the planned motor activity to control a prosthetic arm (Chapin et al. 1999, Kim 2008, Mussa-Ivaldi and Miller 2003). The signals deteriorate with chronic implantation in the brain due to glial scar formation (Polikov 2005 et al.). PNS interfacing, which is less invasive compared to BMI, is the implantation of multi-electrodes in a peripheral nerve of the remnant amputated limb to control the prosthesis. Peripheral neural interfacing is more beneficial and applicable in case of traumatic injury related amputations and may not be effective for amputees affected by diabetic neuropathy where peripheral nerves are damaged.

1.2.8 Insertion mode-based classification of PNS interfaces

Neural interfaces are categorized based on the insertion modes as Penetrating and Regenerative implants [Figure 1.8]. Penetrating arrays are inserted in intact nerves to pierce through the epineurium and contact individual fascicles. These include Utah Electrode Array (UEA), Utah Slanted Electrode Array (USEA), Longitudinal Intrafascicular electrode (LIFE), Transverse Intrafascicular multichannel electrode (TIME). Regenerative arrays include Sieve electrode, Regenerative Multielectrode Neural Interface (REMI). In this mode of insertion, the array is placed in the path of a regenerating nerve. Penetrating and Regenerative modes of implantation are intraneural or intrafascicular method of interfacing. Another approach of implantation is extraneural i.e. implanted around the nerve. Cuff electrodes are implanted

extraneurally, where the electrodes envelop the nerve to record from the fascicles (Navarro et al. 2005).

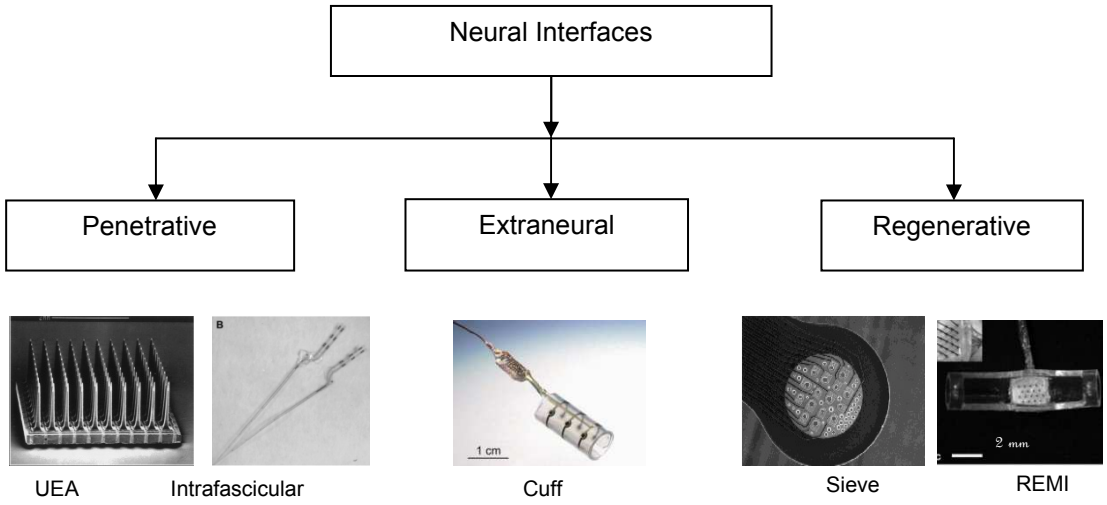

Figure 1.8 Classification of Neural interfaces based on the mode of implantation: Penetrative includes Utah Electrode Array (Maynard et al. 1997), Intrafascicular electrode (Lago et al. 2007), Cuff electrode (Hassler et al. 2011), Regenerative electrodes include Sieve electrode (Mensinger et al. 2000), Regenerative Multielectrode Interface REMI (Garde et al. 2009)

Utah electrode arrays (UEA) and Utah Slanted Electrode arrays (USEA) are high-density silicon probes with 100 micro-electrodes on 4 mm X 4 mm silicon substrate. UEA has electrode shafts of the same length (1 mm) whereas USEA has shafts with gradually increasing lengths (0.5 to 1.5 mm). USEA electrodes are capable to contact neurons in more number of planes compared to UEA, thereby decreasing the number of redundant electrodes and offering three-dimensional access and a better selectivity (Branner et al. 2001). UEA and USEA are implanted into the nerve using a pneumatic actuated insertion tool. In this insertion technique, the electrodes are inserted into an intact nerve at a velocity of 8 m/s. This method of insertion causes initial traumatic injury at the electrode sites (Rennaker et al. 2005). Due to mismatch in the Young's modulus of Silicon electrodes (130-185 GPa) and that of peripheral nerve tissue (66-266 kPa) tissue injury is caused by micromotion over chronic implantations (Pfister et al. 2004).

Longitudinal Intra Fascicular Electrodes (or LIFE) are implanted within individual nerve fascicles longitudinally [Figure 1.9 (B)] (Lago et al. 2007, Badia et al. 2011). Though LIFE electrodes have highly flexible wire design and excellent selectivity, implanting multiple LIFE electrodes in different fascicles is difficult, and therefore, challenging to selectively stimulate various nerve fibers innervating different muscle groups (Malstrom et al. 1998, Branner et al. 2001). Transversal Intrafascicular Multichannel Electrodes (TIME) are implanted transversally in the nerve and contact more number of fascicles [Figure 1.9 (A)], thereby overcoming the limitation of LIFE (Badia et al. 2011). LIFE and TIME are more invasive than Cuff electrodes but provide higher selectivity.

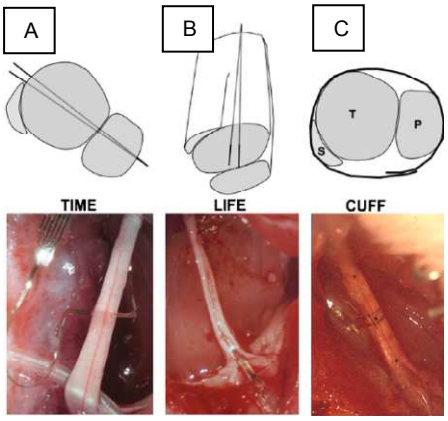

Figure 1.9 Implantation methods of (A) TIME, (B) LIFE and (C) Cuff electrodes (Badia et al. 2011)

Cuff electrodes do not penetrate into the nerve, therefore are less invasive than other methods. This type of electrodes wrap around the nerve and record from the surface of the nerve [Figure 1.9 (C)], Neuropathy due to compression can be inhibited by designing the tube diameter to be 20% larger than the diameter of the nerve (Hoffer 1990). Since Cuff electrodes are extraneural, they have reduced selectivity, unable to eliminate EMG noise and can record from or stimulate only the superficial nerve fibers (Badia et al. 2011).

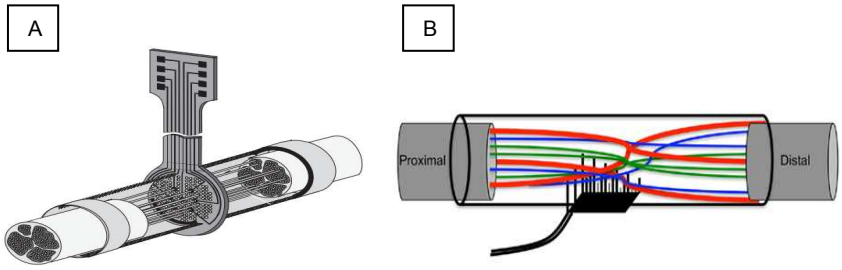

Figure 1.10 Regenerative electrodes: (A) Sieve electrode (Navarro et al. 2005), (B) REMI (Lotfi et al. 2011)

Regenerative interfaces are implanted by placing the electrodes in the path of regenerating neurons to maximize contact with nerve fibers. Sieve electrodes consist of an array with perforations to allow the growing axons to traverse and recording from individual axons [Figure 1.10 (A)]. However, the holes in the array cause constrictive axonopathy for large diameter axons and prohibit normal myelination (Navarro et al. 2005). A recent design of regenerative implantation provides a non-obstructive path where the axons traverse across the FMA [Figure 1.10 (B)]. The Regenerative Multielectrode Interface (REMI) reduces axonopathy and provides a possibility for segregation of neuron types to allow selective stimulation or sensory feedback (Lotfi et al. 2011). Regardless of the mode of implantation, a decline in the number of recording sites is observed with chronic implantation.

1.2.9 Current Limitations

With recent advancements, the neural prosthetics have been enhanced to maximize comfort and performance by fabricating the devices to be light-weight, by improving the ease-of-use, by augmenting the degrees of freedom in case of upper limb prosthetics and by enhancing the socket-fit (Pezzin et al. 2004). However, the following three major limitations still persist– lack of proprioceptive feedback, invasiveness and most importantly, the lack of long-term reliability.

1.2.9.1 Lack of Proprioceptive feedback

Most of the current techniques for prosthetic use are capable of controlling a device by conscious thought process but lack proprioceptive feedback. Methods like myoelectric based

prosthetics depend solely on visual information for maneuvering of the artificial limb leading to user-fatigue and errors in judgment. It requires training for the user to get accustomed to relying on only visual feedback for performing stable prehension (Light et al. 2002). Current prosthetics need to be enhanced by providing sensory feedback (tactile as well as proprioceptive information) (Behrend et al. 2011).

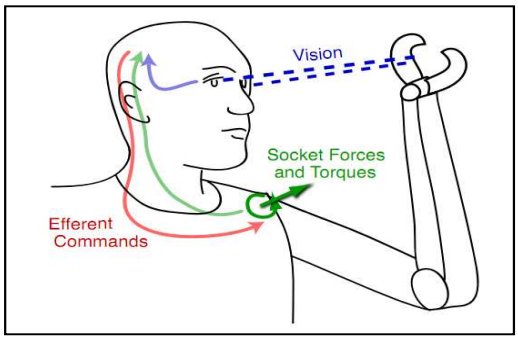

Figure 1.11 Visual feedback-based powered prosthesis where user does not receive proprioceptive information (Kuchenbecker et al. 2007)

Electrodes can be implanted in the peripheral nerve fascicles to establish a two-way communication for better mimicking of natural motor functions. By stimulation of the implanted electrodes, grip force and joint position information can allow the user to better judge the speed and force for modulation of the device (Dhillon and Horch 2005). Segregation of mixed sensory axons in the peripheral nerve is achievable by supply of the appropriate growth factors, thereby allowing selective stimulation of different sensory modalities (Lotfi et al. 2011).

1.2.9.2 Invasiveness versus Selectivity

The spatial selectivity of the electrodes i.e. the ability to record from smallest nerve unit, increases with invasiveness of the technique [Figure 1.12]. While deciding on a technique for measuring neural activity, it is important to weigh the risks involved in the implantation compared to the benefits of the implant and optimize to obtain adequate selectivity with minimum invasiveness (Hassler et al. 2011). Insertion of implants into the nervous tissue leads to aggravated foreign-body response. Severe inflammation takes place at the site of implantation due to the mechanical mismatch between electrodes and neural tissue.

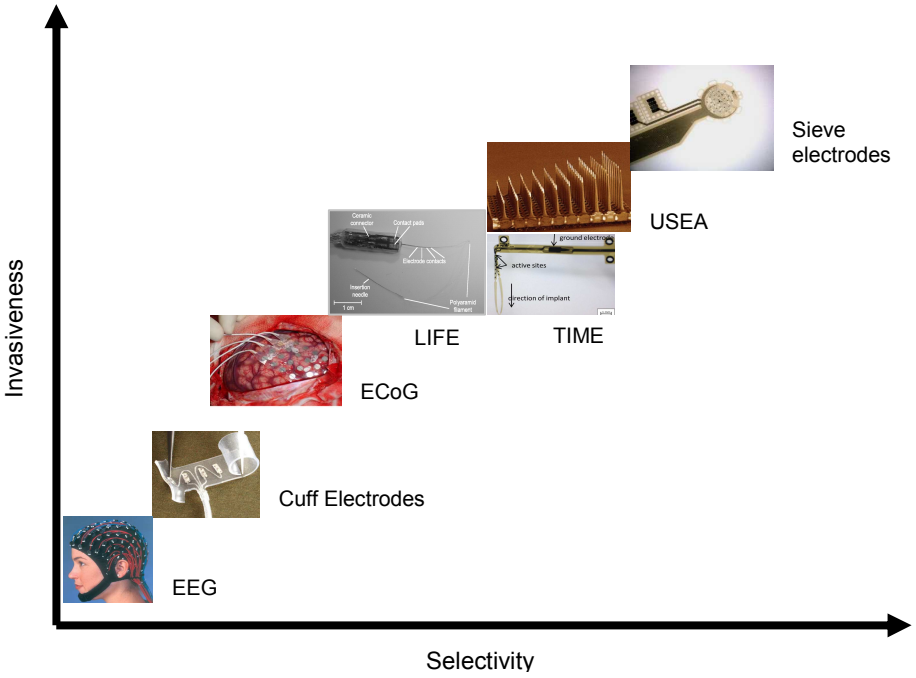

Figure 1.12 Electrodes classified on the basis invasiveness and selectivity (adapted from Hassler et al. 2011)

One method to overcome this issue is to design electrodes of polymer materials with rigidity modulus of similar scale as that of neural tissue (Hassler et al. 2011). Another approach to reduce tissue response due to micro-motion and rigidity mismatch of Young's modulus is tethered implantation. Tethered implantation is to fix the electrodes with respect to neural tissue; hence any movement would be synchronized thereby reducing inflammation due to micromotion.

1.2.9.3 Lack of long-term reliability

Though numerous methods of biocompatible coatings, delivery of anti-inflammatory drugs and neurotrophic factors have been developed (Zhong and Bellamkonda 2005, Cui et al. 2003, Pettingill et al. 2007), a progressive reduction in the number of active sites is seen over chronic implantation. In a study conducted by Rousche and Normann (1998), only 4 of 11 cortical-implanted electrodes could record after 5 months of implantation. A 40% drop in the percentage of active sites was reported by Nicolelis et al. (2003) by the end of 18-month cortical

implantation. In CNS implants, acute response is characterized by recruitment of reactive astrocytes and microglia due to neuron and vascular damage [Figure 1.13 (A)]. Over long-term implantation in CNS, the reactive astrocytes and microglia encapsulate the foreign body to form a glial scar [Figure 1.13 (B)]. The decrease in the ability of electrode to record in CNS over chronic implantation has been associated with this astrogliosis (Schwartz et al. 2006).

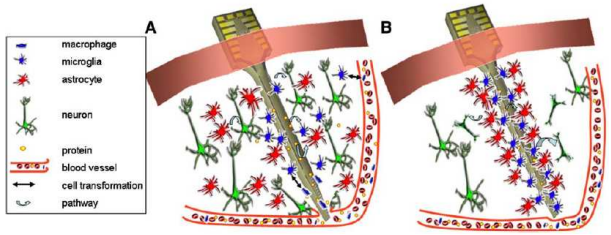

Figure 1.13 Electrode implantation in CNS (A) Acute, (B) Chronic tissue response (Schwartz et al. 2006)

At the end of 7-month study, Branner et al. (2004) reported recordings from only 1 of 7 animals implanted with 100-microelectrode USEA in the sciatic nerve. In a study by Lefurge et al. (1991), six cats were implanted with two longitudinally placed intrafascicular electrodes each in fascicles of radial nerve. At the time of implantation, only 8 out of 12 electrodes could record and a decline of 25% in the percentage of recording electrodes by 4 months post-implantation was reported. In their study, Lefurge et al. (1991) suggested that since 75% of the intrafascicular electrodes were functional 6-months after implantation and the electrode site was well encapsulated in that time-period, the significant decrease in signal-to-noise ratio could not be caused due to inflammatory response. The effect of foreign body response by macrophages on the recording capability of electrodes in PNS implants has not been established yet. Klinge et al. (2001) implanted regenerative sieve electrodes in sciatic nerves of 15 adult Sprague Dawley rats and evaluated CD11+ macrophages around the via hole electrodes after 5 weeks, 6 months and 11 months post surgery. Decrease was reported in the number of hematogenous macrophages after 11 months compared to 5 weeks after implantation. To facilitate

improvement of peripheral implants for long-term application, it is essential to understand the reasons of failure of PNS implants in chronic implantations.

1.3 Specific Aims of the project

Recently a regenerative multi-electrode array (REMI) was developed with an open architecture for the nerve to regenerate, overcoming the limitation of sieve electrode by reducing the axonopathy. A reduction in the number of recording electrodes similar to other neural interfaces is observed in chronic implantations of REMI. This study addresses to evaluate whether the macrophage scar contributes to signal decay in the REMI. To test this hypothesis, two specific aims were considered:

SPECIFIC AIM 1: To investigate if foreign body-tissue response contributes in the decrease of REMI active sites over long-term recordings. The first chapter outlines the characterization of the decline in the number of active recording electrodes over time. The second chapter explains the assessment of the inflammatory response at the electrode sites.

SPECIFIC AIM 2: To determine if electrode micromotion is an important source of continued inflammatory response at the REMI/PNS interface. Chapters three and four detail the evaluation of the nerve injury due to micromotion, outline the main results, and present the possible scope for future experiments.

CHAPTER 2

QUALITY OF NEURAL SIGNAL OVER TIME

2.1 Background

Multi-electrode array interfaced neural prosthetics can achieve natural dexterity in performing motor tasks than primitive methods of body-powered or electric-controlled artificial arms. Neural prosthetic control can be achieved by decoding the electrical signals from the brain or the nerves and by using algorithms to translate this neural activity into motor functions. However, long-term reliability is one of the chief challenges for such neural interfacing, thus limiting their clinical viability. With chronic implantation of microelectrode arrays, a progressive decline in the number of active recording sites has been observed (Polikov et al. 2005, Warwick et al. 2003, and Branner et al. 2004). Reactive astrocyte scarring has been established as the cause of signal attenuation in central nervous system (CNS) implants (Schwartz et al. 2006). However, a conclusive study has not been carried out to ascertain the role of macrophage scar formation as a reason for deterioration of recorded signal in peripheral nervous system implants (PNIs). Unlike other peripheral regenerative electrode arrays like sieve electrode, the array-conduit assembly in Regenerative Multielectrode Interface (REMI) provides a non-obstructive path for regeneration of peripheral nerve; thereby decreasing axonopathy. Since the immune systems of CNS and PNS are dissimilar, the factors causing decrease in functional electrodes of PNS implant REMI need to be investigated. To achieve this, it is essential to characterize the signal decay over time and correlate histological information with this decrease. Electrophysiology was performed by implanting REMIs in the peripheral nerve of a rat for 15, 30 and 60 days followed by histological evaluation, to study the cellular and molecular response to the REMIs over time.

2.2 Methods

2.2.1. Regenerative Multielectrode-Array Neural Interface (REMI) Assembly

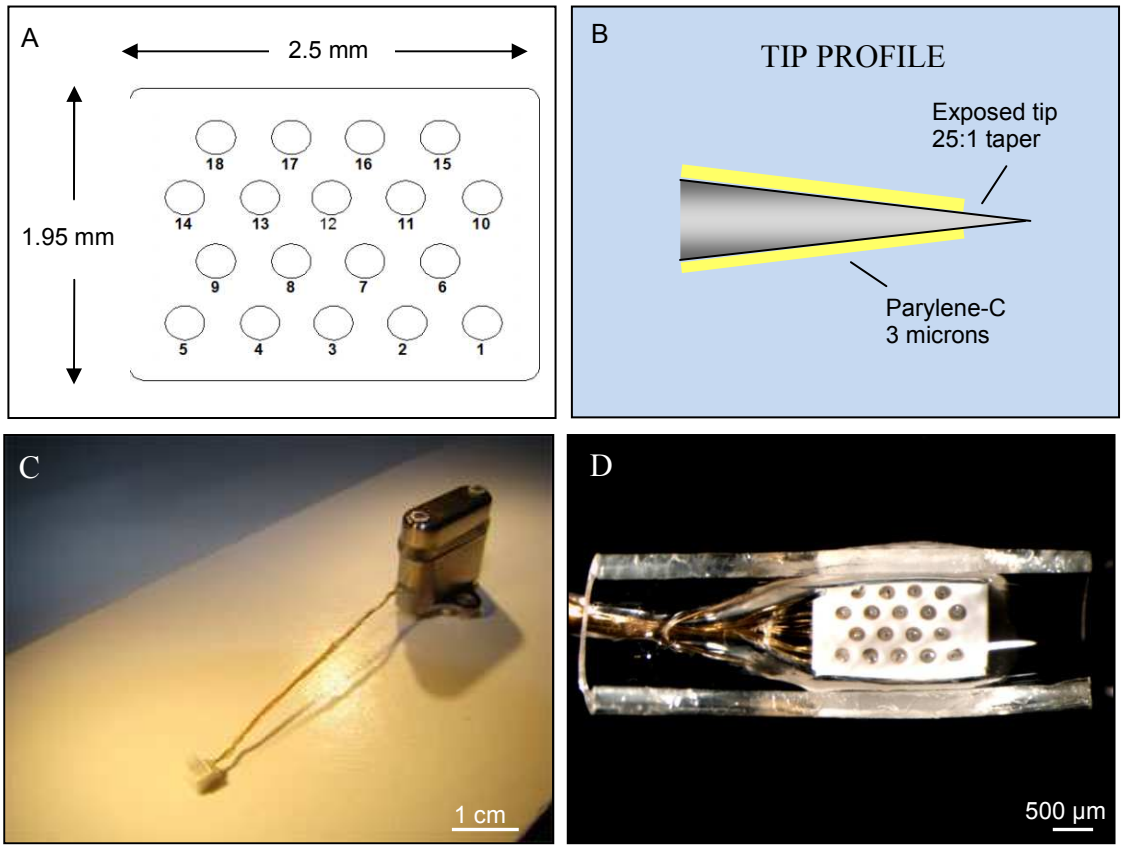

Figure 2.1 Regenerative Multi-electrode neural Interface (REMI): (A) Configuration of 18 electrodes and the dimensions of the Floating Multielectrode array, (B) Schematic representing the electrode tip profile and Parylene-C insulation, (C) Titanium pedestal encasing an Omnetics connector linking the microelectrodes via Parylene-C coated gold wires, (D) An 18-pin Floating Multielectrode Array placed in a 7 mm Polyurethane tube

REMI comprises a Floating multielectrode array (FMA) placed in the lumen of a polyurethane tube. FMAs were custom made having the dimensions of 2.45 mm X 1.95 mm X 0.45 mm (Microprobes Inc., MD) [Figure 2.1 (A)]. Each FMA consists of 18 Platinum/Iridium (70/30%) electrodes which are separated by 400 µm. Pt/Ir electrodes provide low noise characteristics. The impedance of the electrodes range between 150 kΩ to 300 kΩ tested at 1 kHz i.e. in the neuronal spike range (Schmidt et al. 1988). The heights of the electrode shafts vary between 0.7 mm to 1 mm to maximize contact with more number of neurons in different

planes. The electrodes are coated with Parylene-C except at the tip, to provide insulation and expose only a small surface area (2-3 μm) enabling recording from smallest individual neurons [Figure 2.1 (B)]. The microelectrode shafts have a base diameter of 50 μm and the shafts are linked to the Omnetics connector via Parylene-C insulated gold wires having 25-micron diameter. The gold wires (4.5 cm in length) are wound in a helix and coated with a NuSil-type MED6-6606 non-restrictive silicone elastomer for durability and flexibility. The Omnetics connector is housed in a Titanium pedestal which serves as an external interface for recording [Figure 2.1 (C)]. The pedestal prevents the connector contacts to be exposed to moisture and external debris by employing a silicone gasket and a titanium lid. The 7 mm-long polyurethane conduit with outer diameter of 3 mm and inner diameter of 1.75 mm (Micro-Renathane®, Braintree Scientific, Inc.) holds the FMA [Figure 2.1 (D)]. The polyurethane nerve guide is filled with collagen I/III (0.3%; Chemicon, Temecula, CA, USA) and is sterilized a day prior to the surgery by Ultraviolet radiation.

2.2.2. Surgery and implantation

Thirty female Lewis adult rats (200-275g) were used in this study (n=6 for REMI-implanted and n=4 for Control, for three time-points: 15-day, 30-day and 60-day). The animals were anesthetized with Isoflurane (5% induction, 2.5% maintenance) in 100% oxygen. The eyes were kept moist using an ophthalmic ointment. The dorsal side of the pelvic and the left thigh regions were shaved after the animal reached adequate level of anesthesia indicated by loss of corneal reflex). 70% Ethanol and Povidone-iodine were applied to the surgical site for disinfection.

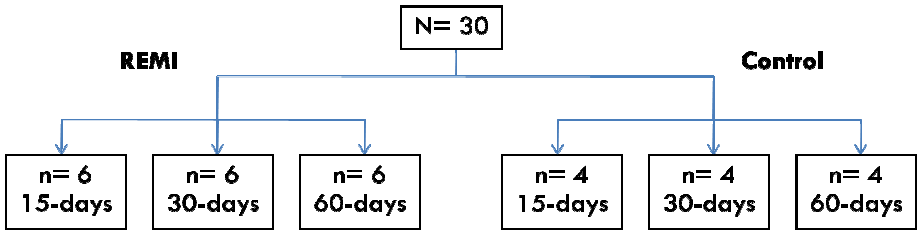

Figure 2.2 Schematic showing subject classifications

A vertical incision was made through the skin in the pelvis region; the fascia was reflected and the underlying muscle tissue was cleared. The tips of the exposed dorsal processes were removed and the pedestal was mounted on the pelvis. Bone cement (Biomet; Warsaw, Indiana, USA) was applied around the pedestal to hold it in place [Figure 2.3 (A)]. The array and the gold wires linked to the connector were passed subcutaneously to the biceps femoris muscle.

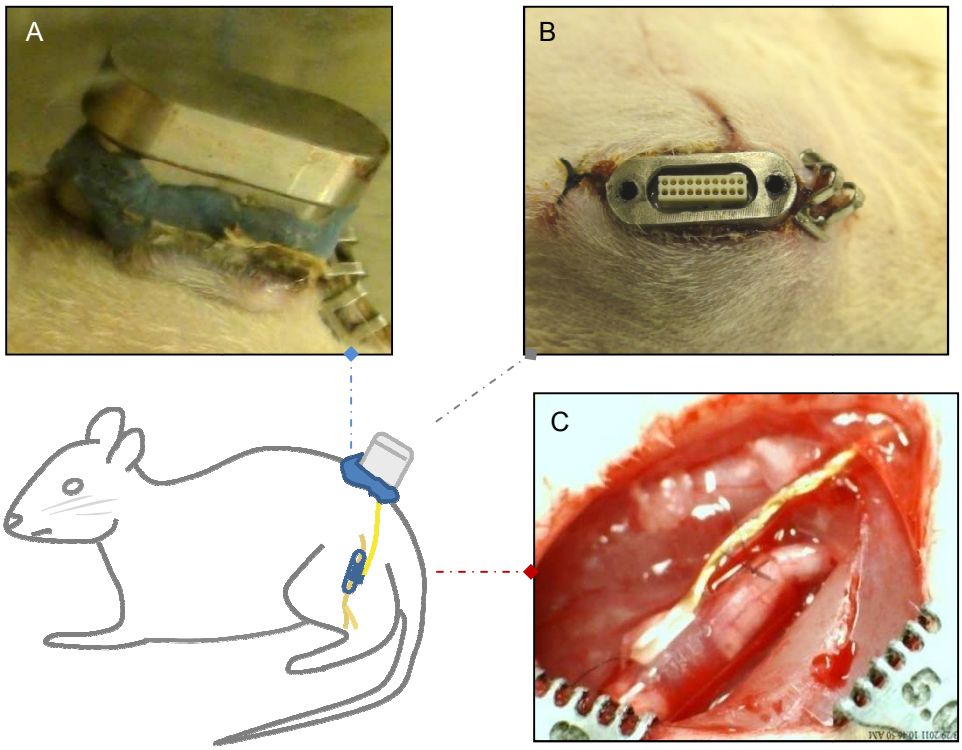

Figure 2.3 Schematic illustrating implantation of Regenerative Multielectrode Neural Interface (REMI) in left hind limb of a rat: (A) Bone cement used to secure the pedestal to the pelvis, (B) Titanium Pedestal housing the Omnetics connector, (C) REMI sutured to the sciatic nerve stumps

A vertical incision was made on the left thigh and the fascia was cleared. The biceps femoris and the semitendinosus muscles were spread apart; the sciatic nerve was exposed and then transected. The proximal and the distal stumps of the nerve were inserted in the ends of the sterilized REMI conduit. The nerve endoneurium was sutured to the tube ends using 10-0,

140 µm mono-filament suture [Figure 2.3 (C)]. The muscles were sutured together with a 3-0 chromic gut suture and the skin was stapled together at the REMI and the pedestal implanted sites [Figure 2.3 (B)]. The animals were applied with antibiotic ointment (Fougera, Triple antibiotic Ointment) on the surgical site. After regaining consciousness, the animals were injected with antibiotic (Cefazolin, 5 mg/kg) intramuscularly on the contralateral thigh and with pain control (Buprenorphine, 0.1 mg/kg) subcutaneously at the dorsal side of the neck. The procedure for Control animals was performed using collagen-filled tubes without the FMA and did not involve pedestal implantation. The surgical procedures were carried out in accordance with the guidelines of Institutional Animal Care and Use Committee (IACUC) of the University of Texas at Arlington.

2.2.3. Data Acquisition

The neural activity was recorded weekly from the eighteen REMI-implanted animals by Omniplex data acquisition system (Plexon Inc., USA). The set-up for carrying out electrophysiology from the regenerating nerves in freely moving rats is shown in the Figure 2.4 (A) & (B). Op-amp based unity-gain headstage amplifier was used to connect the Omnetics connector to the amplifier as shown. The headstage pins for reference and ground are used differentially at the preamp level. The amplifier provides high signal-to-noise ratio (SNR), good common-mode rejection ratio (CMRR) at 0-60 Hz (>100 dB), programmable reference channel, programmable gain from 250X to 8000X gain and 4-pole Bessel analog high-cut filter at 8 kHz. The programmable selection of reference channel allows effective elimination of artifacts due to noise and interference before further processing of the information. The amplifier was connected to the signal processing chassis via a ribbon cable. The system processes the data for analog to digital conversion (16-bit A/D) at 40 kHz. The Omniplex chassis is connected to a computer for real-time monitoring of the neural activity and for adjusting the parameters as required. The neural signals were recorded from 16 channels of the REMI (gain set at 8000X) for 1 minute from the rat in anesthetized state and for 5 minutes when in wake state.

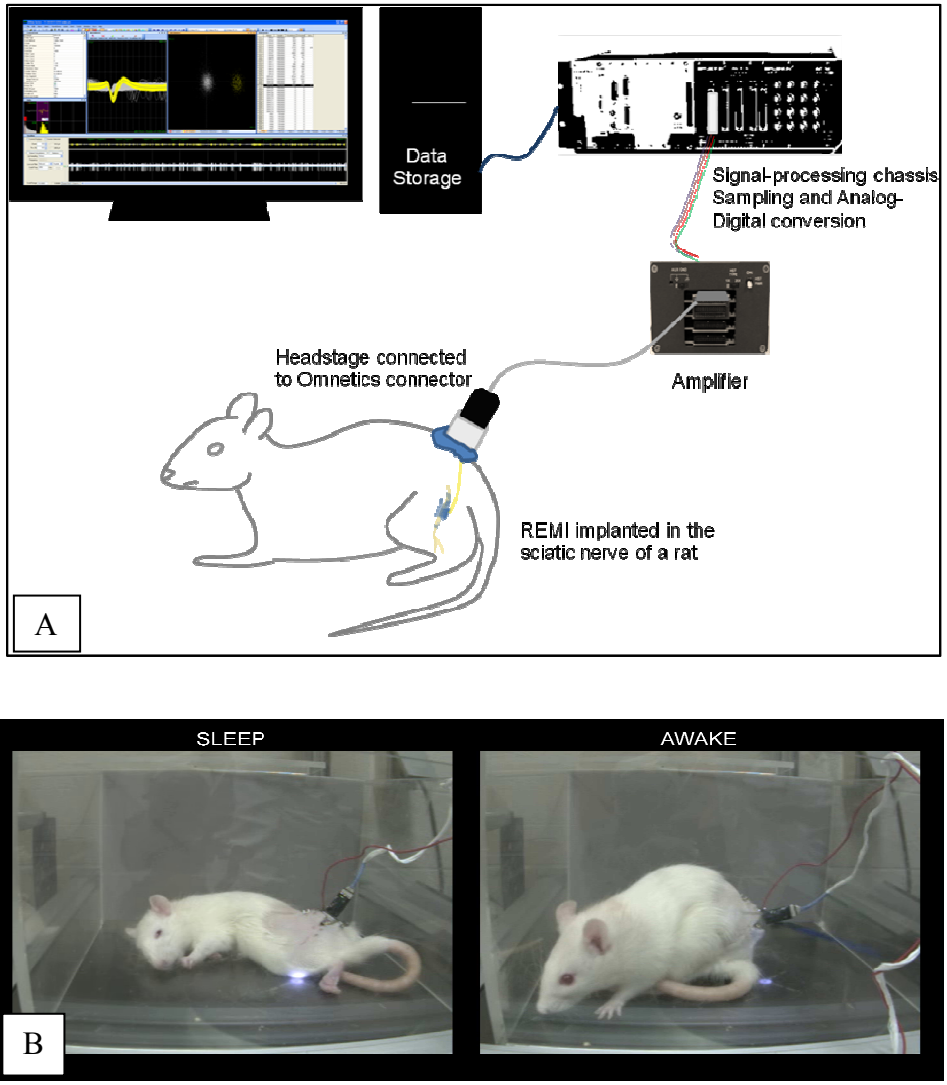

Figure 2.4 (A) Schematic showing the set-up for electrophysiological recording: acquisition and storage of neural signals, (B) for 1 minute in anesthetized state and 5 minutes in wake state

2.2.4. Data Analysis

The data acquired was processed for spike sorting using Offline Spike Sorter (Plexon Inc., USA). Signals from the sixteen channels were filtered using an 8-pole Bessel high-pass filter at 300 Hz to eliminate the low-frequency motion artifacts and power-line interference (Figure 2.5) (Logothetis 2002, Quiroga et al. 2004). Offline Sorter displays the data for

waveform detection as histogram of the logarithm of peak heights [Figure 2.6 (A)]. The filtered data which lies in the frequency range of 300 Hz to 8 kHz was then thresholded based on the amplitude by selecting waveforms above the three sigma noise level [Figure 2.6 (B)].

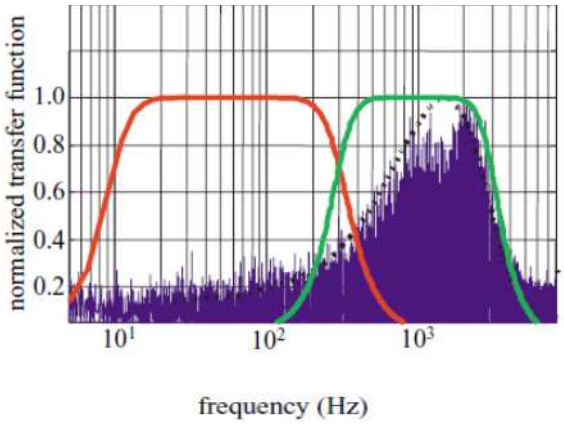

Figure 2.5 Filter transfer functions: Red trace representing Local Field Potential filter transfer function, Green trace showing Unit Spike transfer function, Blue plot showing range of single unit spikes from 300 Hz to 3000 Hz (Logothetis 2002)

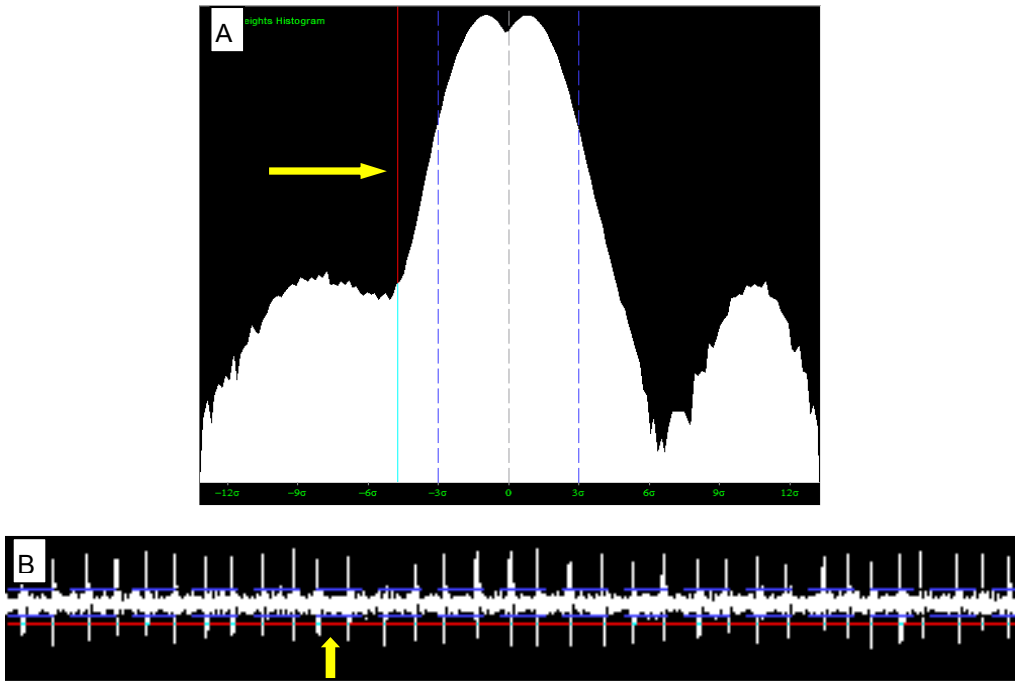

Figure 2.6 (A) Histogram of peak heights with dashed blue lines representing three-sigma noise level and red line indicating the threshold level (yellow arrow), (B) Recorded activity with the three sigma noise level blue dashed lines and threshold level (yellow arrow)

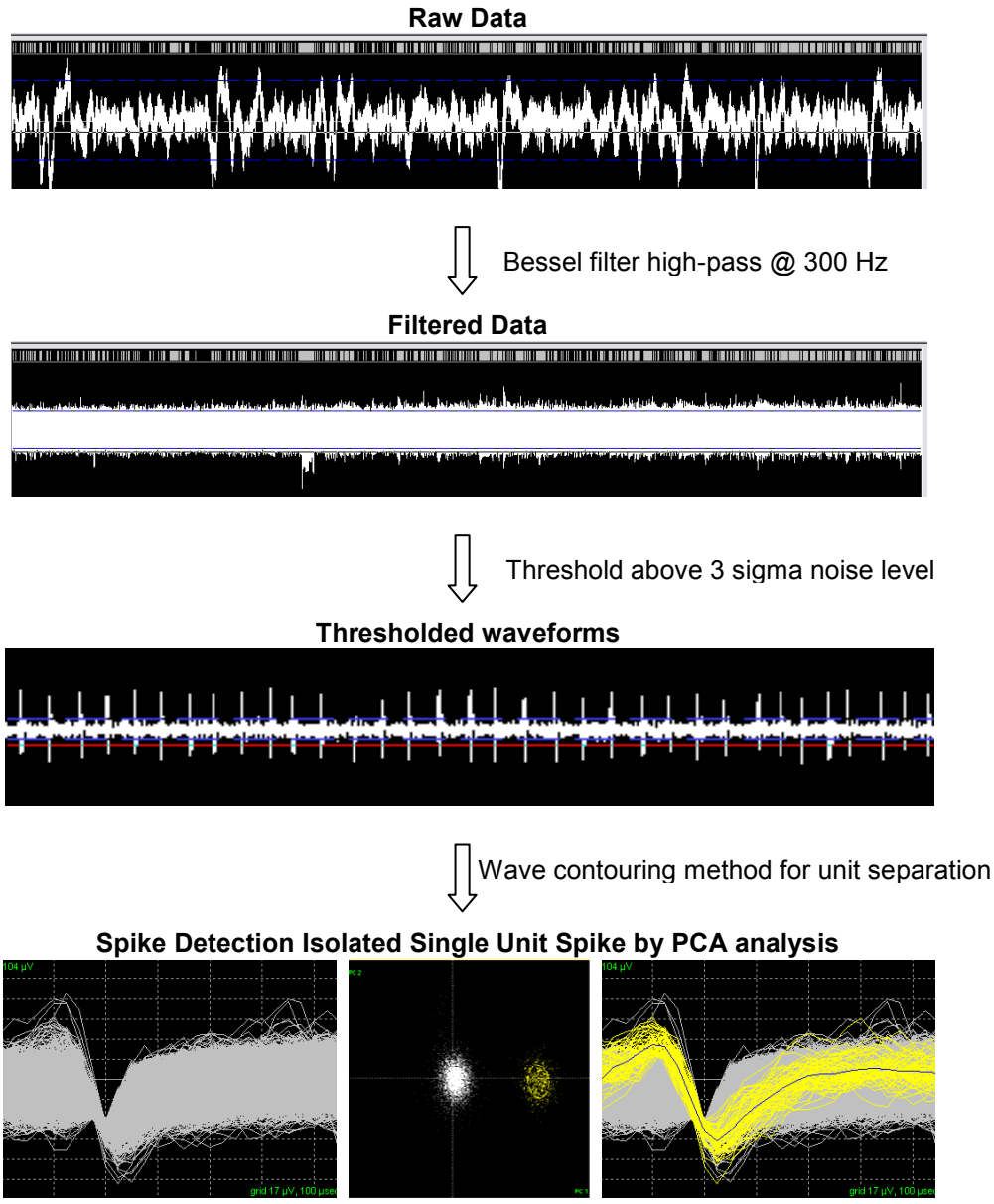

Figure 2.7 Steps for sorting and extraction of Single Unit Spikes (adapted from Quiroga et al. 2004)

Spike sorting was performed using 3-component Principal Component Analysis (PCA) to isolate the Single Unit Spikes (SUS) from the noise and the other neural signals. PCA classifies the waveforms associated with different individual or groups of neurons and then projects the formed clusters in orthogonal planes [Figure 2.7]. A unit, representing a group of SUS from the same set of neurons, can be detected using waveform contouring method from

the PCA separated clusters. The amplitude and the noise baseline were quantified using envelope detection method in MatLab.

2.3 Results

All thirty animals survived the surgery and the eighteen REMI-implanted rats were subjected to weekly electrophysiological recordings. Data was acquired from animals for 1 minute when in anaesthetized state to collect baseline noise information. Another 5 minutes of electrophysiology was performed from conscious and freely moving animals without any application of external stimulus. The animals were sacrificed after 15, 30 and 60 days post-implantation (N=6 at each time-point) for histology. Single Unit Spikes (SUS) were detected earliest at 7-days post-injury from two of the eighteen implanted animals. Of the six 60-day animals, neural activity was recorded from only one animal at the final time-point of weekly recording i.e. 56-days after implantation. Multiple units on single channel were recorded from 1 animal on day 14, from 5 animals on day 21, from 1 animal on day 28 and from 1 animal at day 35. In the entire study, maximum number of channels recording single unit spikes was 7 out of 16 electrodes on day 21 post-implantation with detection of 11 distinct units. All the sorted single unit spikes had amplitudes in the range of 38.71 to 404.62 μV and signal-to-noise ratio in the range of 0.59:1 to 7.98:1. Two 60-day animals could not be recorded from after 30-days of surgery due to failure by detachment of pedestal.

2.3.1. Quality of neural activity recorded from day 7 to day 56

Figure 2.8 shows single unit sorting using PCA analysis and waveform-contouring method with each cluster color-coded to represent a distinct unit. Amplitudes were measured using envelope detection for each recorded unit and recorded baseline noise on the corresponding channel at different time-points. Noise did not show significant difference among the time points. Signal-to-noise ratio (SNR) was measured as ratio of the unit amplitude peak-to-peak to baseline noise amplitude. Graph in Figure 2.9 shows the amplitude (μV) of unit spikes from day 7 to day 56 post-surgery time points with the error bars representing standard

error mean. One-way ANOVA was performed to compare amplitudes at different time-points and Newman Keuls method was used to perform multi-group comparisons. 56-day time point was excluded from the statistical tests since activity was recorded from only one animal at this time-point. No significant difference was observed in the amplitudes between any of the time-points. Images of single unit spikes with the maximum amplitude recorded on each time-point (7 to 56) are shown in the Figure 2.10 (A-G).

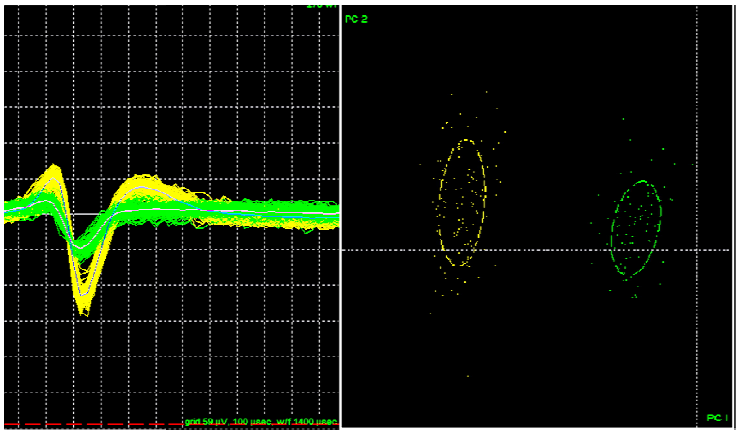

Figure 2.8 Illustration of Wave-contouring method for sorting of single unit spikes

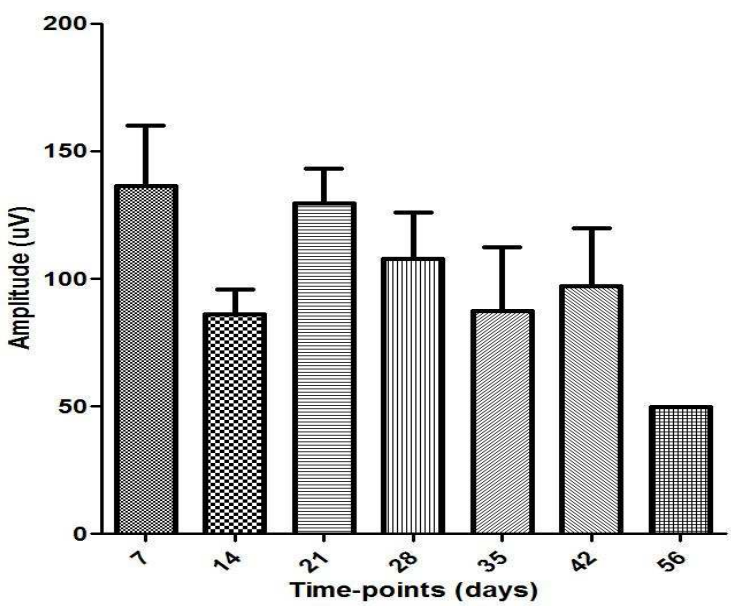

Figure 2.9 Amplitude of Single Unit Spikes recorded at weekly time-points of day 7 to day 56 post-implantation

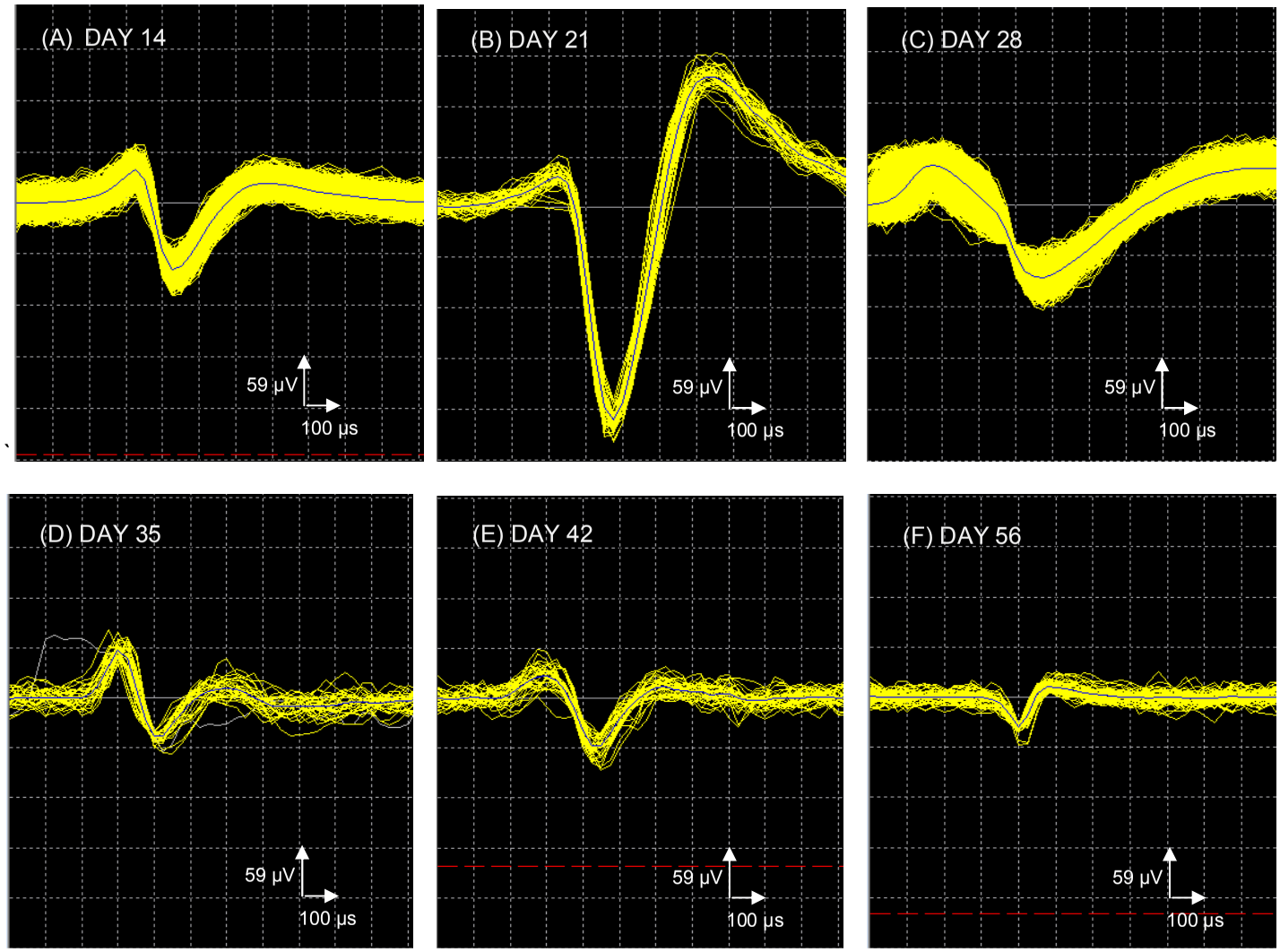

Figure 2.10 Single Unit Spikes with maximum amplitude recorded at time points (A) 14 days, (B) 21 days, (C) 28 days, (D) 35 days, (E) 42 days and (F) 56 days after implantation

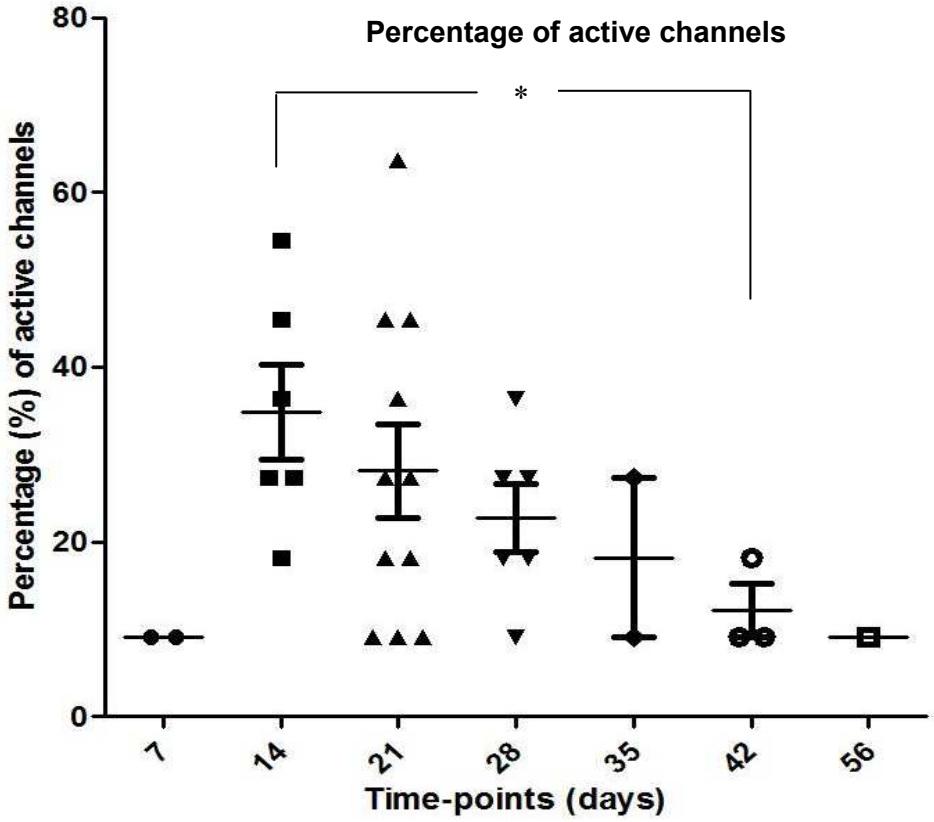

Figure 2.11 Decline in the percentage of active electrodes per implanted array with the weekly time-points is shown in the graph

Percentage of active channels over 7 to 56 days post-surgery is shown in Figure 2.11. This data was compared by one-way ANOVA. 56-day time point is not included due to sample size of one. A significant reduction was observed in the percentage of recording electrodes from 14 days to 42 days. Histological evaluation was carried out following electrophysiology to correlate tissue response with the decrease in percentage of functional electrodes.

2.4 Discussion

Decrease in percentage of recording electrodes over chronic implantation of neural interfaces has been well established for central nervous system (Nicolelis et al. 2003, Polikov et al. 2006). This decline is caused due to the foreign body response or glial scar formation at the site of implantation. Micro-electrodes are capable of recording from single neurons which are in close proximity. However, foreign body reaction or astrogliosis increases the distance between

the electrode and the neuron; thereby reducing the ability of the electrode to record. Though a similar tendency of reduction in active electrodes is seen in peripheral implantations (Warwick et al. 2003, Lefurge et al. 1991), the cause has not been established. Based on qualitative analysis, Garde et al. (2009) reported decrease in the amplitude recorded from sciatic nerve implanted REMI from day 8 to day 46 post-implantation. This study was carried out to assess electrophysiological signals over long-term implantation and correlate the quality of signals with histological changes. Eighteen rats were implanted with regenerative neural interface that provides a non-obstructive conduit for axons to regenerate. We found no significant change in the amplitude or signal-to-noise ratio between any time-points. However, separate analysis of the maximum action potential amplitude values recorded on each time-point revealed a three-fold decrease from 21 to 42 days post-implantation. A significant reduction in the percentage of electrodes recording single action potentials was also observed from 14 to 42 days post-implantation. In regenerative mode of implantation, the sciatic nerve is transected and the FMA is placed in the path of axon regeneration. Since the REMI requires nerve transection for implantation, a strong injury-induced inflammatory response mediated primarily by macrophages is expected. Thus, macrophage scar formation around the electrodes is likely a major factor in the reduction of signal detection by the REMI over time. From the prior studies on chronic implantation, the role of scar formation in reduction of number of active sites has been shown to play a critical role in CNS implants. Amplitude attenuation with chronic implantation suggests insulation of the functional electrode tip which could be a result of FMA elicited foreign-body response at the electrode site (Polikov et al. 2005, Polikov et al. 2006, and McConnell et al. 2007). To confirm and understand the function of scar at PNS interface location in decrease of percentage of active electrodes, tissue response at the site of implantation and the dynamic microenvironment is evaluated. Macrophage scar at the electrode site was quantified and compared at the three time-points 15, 30 and 60-day post-injury.

CHAPTER 3

EVALUATION OF INFLAMMATORY RESPONSE AT ELECTRODE SITE

3.1 Background

Deterioration in quality of signal recorded from neural interfaces with chronic implantation has been associated with tissue damage at interface, foreign-body response and glial scar formation in CNS (Polikov et al. 2005). In peripheral implants, this relation has not been well established. REMI implanted rat sciatic nerves were harvested at 15, 30 and 60 days after surgery and processed for immunofluorescence. Sections of the sciatic nerve were labeled for ED1 reactive macrophages around the site of implantation. The macrophage scar area and cell density in this area were quantified at different time points. Change in the inflammatory response with time was correlated with the electrophysiological recordings to understand the role of tissue reaction with the decrease in number of functional recording sites in REMI.

3.2 Methods

3.2.1 Sciatic Nerve Harvesting and sample preparation

Eighteen REMI implanted animals and twelve control rats implanted with collagen-filled polyurethane tubes (i.e., no FMA), were sacrificed after 15 days, 30 days and 60 days post-implantation (n=6 REMI and n=4 control animals for each time point). The animals were euthanized via an intraperitoneal injection of sodium pentobarbital (100 mg/kg) and sacrificed by transcardial perfusion with 0.9% saline for 5 minutes followed by 4% Paraformaldehyde (PFA) for 15 minutes. The regenerated nerve is harvested along with the polyurethane tube, post-fixed overnight in 4% PFA and then transferred to 1X PBS (Phosphate Buffered Solution). The tube, holding the FMA was removed carefully [Figure 3.1 (A, B and C)]. The proximal and the distal ends were marked with green and red dyes respectively. The orientation of the electrodes was marked using blue dye [Figure 3.1 (D)]. The nerve was embedded in paraffin wax for histology.

The paraffin-embedded nerve sample was sectioned at 6 µm thickness and mounted on positive-charged slides.

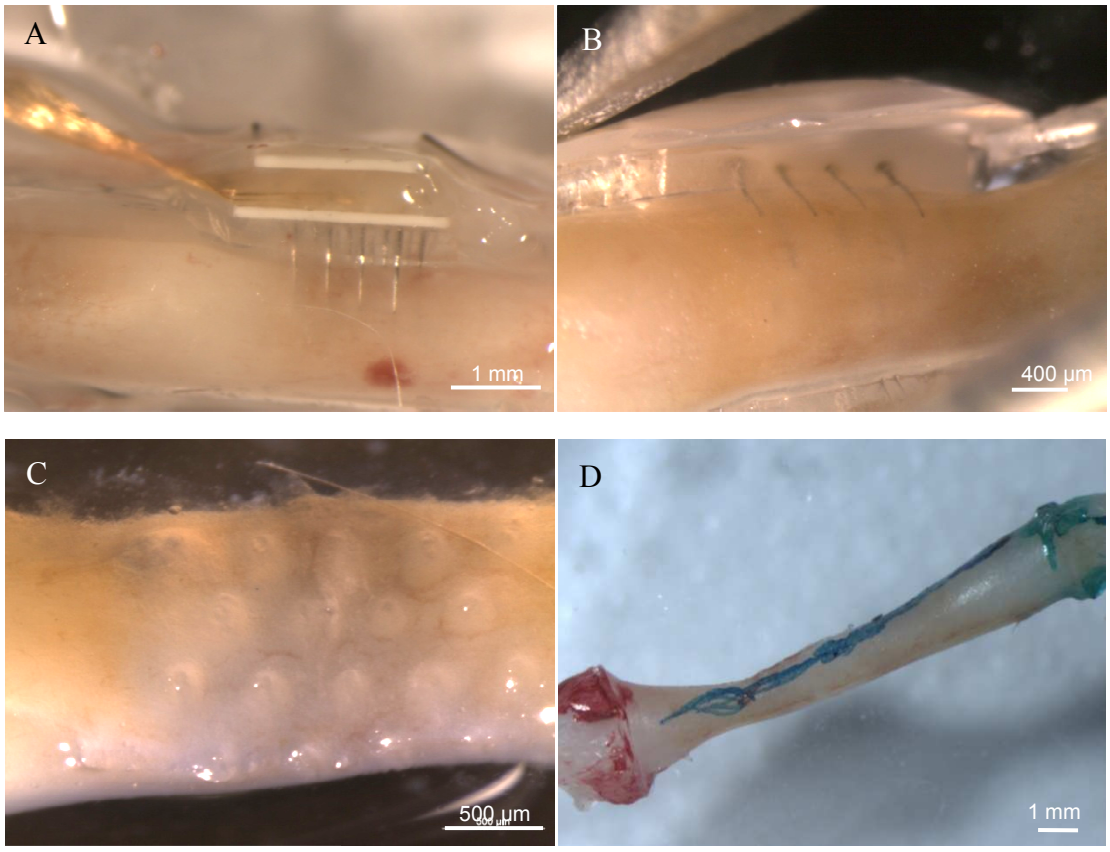

Figure 3.1 Sample preparation: (A) Harvested REMI-implanted Sciatic nerve covered with fibrous tissue, (B) REMI implanted nerve with Polyurethane tube removed showing penetrating electrodes, (C) Perforations left by electrodes, (D) Nerve marked with dyes to mark proximal (green), distal (red) and electrode orientation (blue) processed for paraffin embedding

3.2.2 Immunofluorescence staining

The paraffin sections were placed in an oven at 58-60° C for 30 minutes and then deparaffinized with two changes of xylene for 5 minutes. The sections were hydrated by dipping them in descending grades of alcohol – twice in 100% ethanol for 3 minutes, once in 90% ethanol for 3 minutes, once in 70% ethanol for 3 minutes followed by 1 minute in distilled water. The antigen retrieval was achieved by heating the sections in citrate buffer at 80° C for 15 minutes. The sections were then kept at room temperature in citrate buffer for 20 minutes. The slides were

washed for 10 minutes in 1X PBS. The sections were incubated with 4% normal goat serum (Jackson Immunoresearch) mixed in 0.5% TritonX-100 (Sigma) washing solution (which was made in 1X PBS) for 1 hour to block non-specific binding. After the blocking solution was removed, the sections were washed and incubated in primary antibodies overnight at 4° C. Primary antibodies for macrophages - mouse anti-ED1 (Millipore) were diluted (1:250) in the blocking solution. The slides were washed with three washes of 0.5% TritonX followed by one wash with 1X PBS. They were then incubated for 1 hour in secondary antibodies – Goat anti-mouse IgG Dylight 488 diluted (1:400) in washing solution. The slides were washed, counter stained with DAPI and mounted with mounting medium.

3.2.3 Imaging and Quantification

The ED1 stained sections were imaged using Carl Zeiss, Axiocam. The area of the macrophage scar around the electrode site and the macrophage cell density in the scar area were quantified using the AxioVision Rel 4.8 application. The scar region was defined, area measured and DAPI stained nuclei colocalized with the ED1 labeled cells were counted [Figure 3.2]. The cell density was calculated based on the number of cells in the measured area of the macrophage scar. The quantification was performed on four electrodes for each animal.

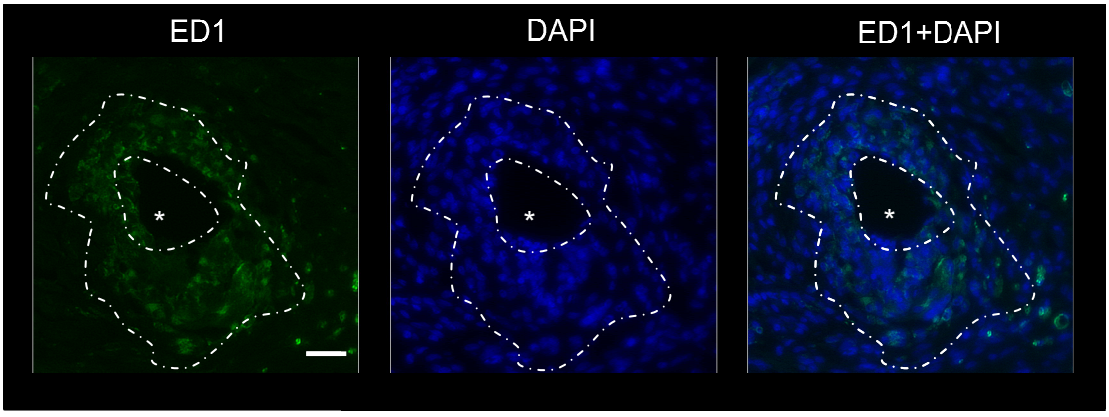

Figure 3.2 Quantification of the area and the cell density of the macrophage scar around the electrode implanted site (denoted by asterisk). Scale Bar = 20 μm

3.2.4 Statistical Analysis

The area and the cell density at 15, 30 and 60 days post-implantation were compared using unpaired student's t-test for unequal variances. With the significance level $\alpha = 0.05$, p-values less than 0.05 were considered to be statistically significant. The results were reported as mean ± standard deviation or mean ± standard error of the mean.

3.3 Results

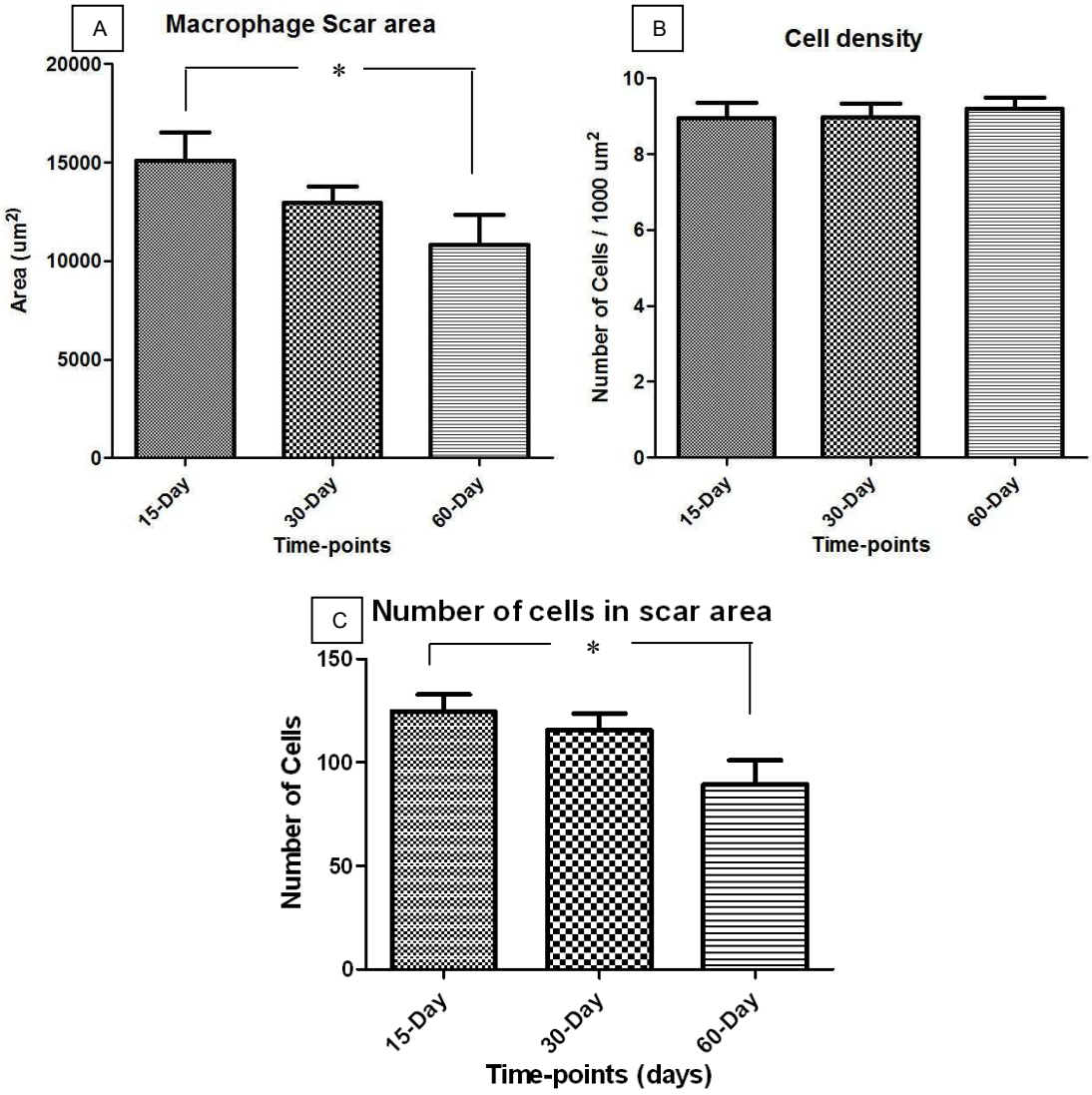

Figure 3.3 Comparison of (A) Macrophage scar area, (B) Macrophage cell density, (C) Number of cells in scar area at 15, 30 and 60 days post-implantation

Harvested nerve samples showed robust nerve regeneration with regenerated nerve filling the entire lumen of the tube at 60-day time point. The polyurethane conduits were enveloped by vascularized fibrous tissue in the explanted nerves of all time points [Figure 3.1 (A)]. The nerve samples were extracted from the tubes [Figure 3.1 (B) & (C)] and processed for histology. Quantification of the tissue response was carried out by measuring the ED1 labeled area and the cell density of reactive macrophages around electrodes at different time points. DAPI stained cells in the macrophage scar area also include fibroblasts which are part of inflammatory response and are devoid of Schwann cells (Garde et al. 2009).

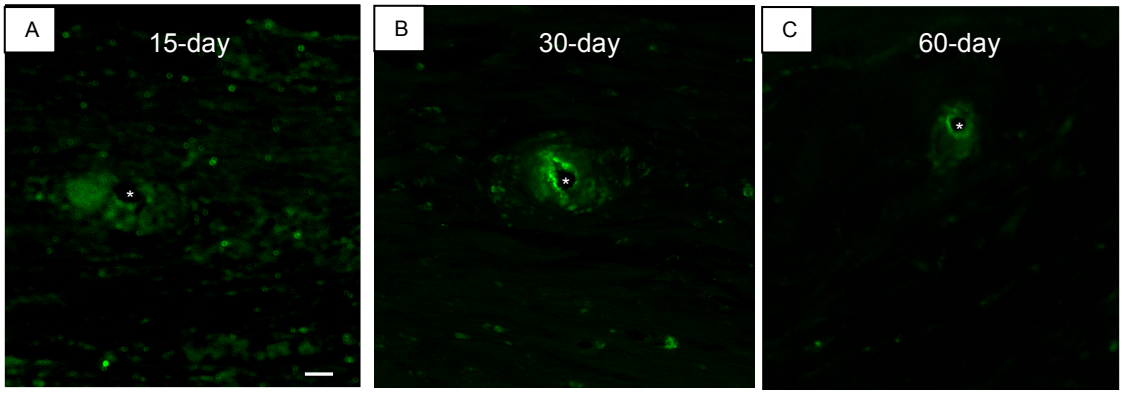

Figure 3.4 Macrophages at electrode implant site: Representative fluorescence images of ED1+ labeled cells at (A) 15-days, (B) 30-days and (C) 60-days after implantation (electrode location denoted by asterisk). Scale bar = 30 μm

Figure 3.3 (A) compares macrophage scar area due to electrode-tissue interfacing, after 15, 30 and 60 days of implantation. A significant decrease was seen in the macrophage scar area from 15-days to 60-days post-implantation. Since the inflammatory response area reduced after 60 days of implantation, cell density of the scar area was measured to test if the scar had compacted. Graph in Figure 3.3 (B) shows the scar cell density at 15, 30 and 60 days post-surgery. No significant difference was seen in the cell density between any of the time points.

3.4 Discussion

Clinical use of multi-electrode arrays to interface neural tissue with prosthetic limb is not viable due to the lack of reliability of such electrodes. Studies have reported decline in the number of active channels with long-term implantations (Polikov et al. 2005, Warwick et al. 2003, and Branner et al. 2004). Tissue response elicited by chronic electrode implantation causes the distance between electrode and neural tissue to increase leading to decay in the capacity of electrode to record. In cortical implants, the astroglial scar becomes more compact with long-term implantation (McConnell et al. 2007). To evaluate the function of foreign body response in decrease in number of active sites with chronic implantation of peripheral regenerative implant REMI, reactive macrophage scar area and cell density around the electrode sites were measured. A decrease in the scar area was observed from day 15 to day 60 post-implantation. This shows reduction in the inflammatory reaction with time. We also confirmed that the cell density of reactive macrophages did not increase between 15-day and 60-day time points, thus illustrating that the macrophage cells do not arrange close together or compact with time. The amplitude and percentage of sites recording neural activity were maximum on day 21 post-operation though macrophage scar due to the tissue response was already present at 15 dpo. A decline in the percentage of active sites was seen after 42 days of implantation suggesting that macrophage scar does not play a role in the reduction of functional electrodes.

CHAPTER 4

EVALUATION OF NERVE INJURY DUE TO MICROMOTION

4.1 Effects of micromotion

Successful chronic implantation of microelectrode array interfaced to the nervous system is dependent on stable contact between electrode and neurons (Thelin et al. 2011). The fixation mode of electrode array plays an important role in maintaining stable contact where failure in interface occurs due to increase in functional distance between electrode and neurons by neuronal loss around the electrode or by exacerbated inflammatory response. When an array is implanted in tethered mode as shown in Figure 4.1 (A), electrode stays in a fixed position. Since the brain moves within the skull cavity more in the anterio-posterior axis than in medial-lateral axis, tethered electrode causes increase inflammatory response leaving an oval shaped cavity representing the brain movements [Figure 4.1 (C)]. In untethered mode of implantation, the electrode moves along with the brain tissue and does not cause the effect of micromotion [Figure 4.1 (B) and (D)].

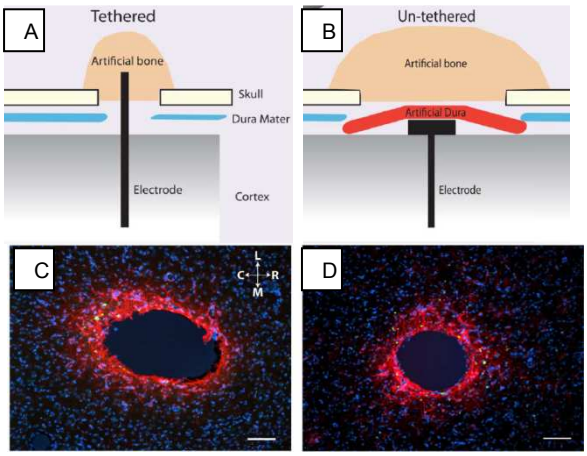

Figure 4.1 (A) Tethered mode of implantation, (B) Untethered mode of implantation, (C) Oval cavity left by tethered electrode, (D) Inflammatory response around untethered electrode (Thelin et al. 2011)

Along with increased inflammatory response, a decrease in the number of neuronal bodies around the electrode has been reported (Biran et al. 2005). In peripheral nervous system, due to daily limb movements stretching of nerve may lead to similar effect of micromotion after electrode implantation. Philips et al. (2004) reported regional heterogeneity of tensile properties of nerve with regions near the joints undergoing higher elongation than the regions away from the joint. A peripheral nerve can move with respect to surrounding tissues by several centimeters which can lead to micromotion effects in a peripheral interface (Sung-Hoon Cho et al. 2008). It is essential to characterize the mode of implantation of regenerative interface REMI and quantify neuronal loss due to micromotion.

4.2 Molecular mechanism in response to Sciatic nerve transection

Nerve injury initiates a complex mechanism of molecular signaling to induce regeneration of the injured neurons in the peripheral nervous system (PNS) or for the retraction of the synaptic terminal of the axotomised neuron in the central nervous system (CNS). The injured axons in the adult CNS lack the intrinsic capacity to regenerate; whereas the peripheral nerves are capable of regeneration. After injury, the retrograde flow of cellular signals to the PNS cell bodies located in the spinal cord and the dorsal root ganglia is disrupted. Calcium influx due to the exposure of the neuron plasma to the external environment (Makwana and Raivich 2005) contributes to a cellular response to injury which includes both morphological and molecular changes which prepare the cell for assimilation of injury and for subsequent regeneration (Liu et al. 2011).

4.2.1 Morphological changes in axotomized peripheral neurons

Following the axotomy, the neurosoma and the axon exhibit distinct responses. Due to the axon disruption, chromatolysis takes place in the neuronal cell body, which is observed as the dispersal of Nissl substance. The soma becomes hypertrophic and the nucleus becomes vesicular and is displaced towards the periphery of the cell. The proximal stump of the neuron is sealed and the cytoskeleton reorganizing occurs allowing the growth cone formation. The distal end of the axon undergoes Wallerian degeneration. The resultant axonal fragments and the

myelin debris are cleared by the recruited macrophages, thus providing a favorable environment for regeneration (Liu et al. 2011). The proximal stump sprouts regenerative axonal buds (Chen et al. 2007) [Figure 4.2 (B)]. Schwann cells that lose contact with the axon proliferate and align with the endoneurial tubes forming bands of Büngner, serving the purpose of regenerative substrate [Figure 4.2 (C)] (Deumens et al. 2010).

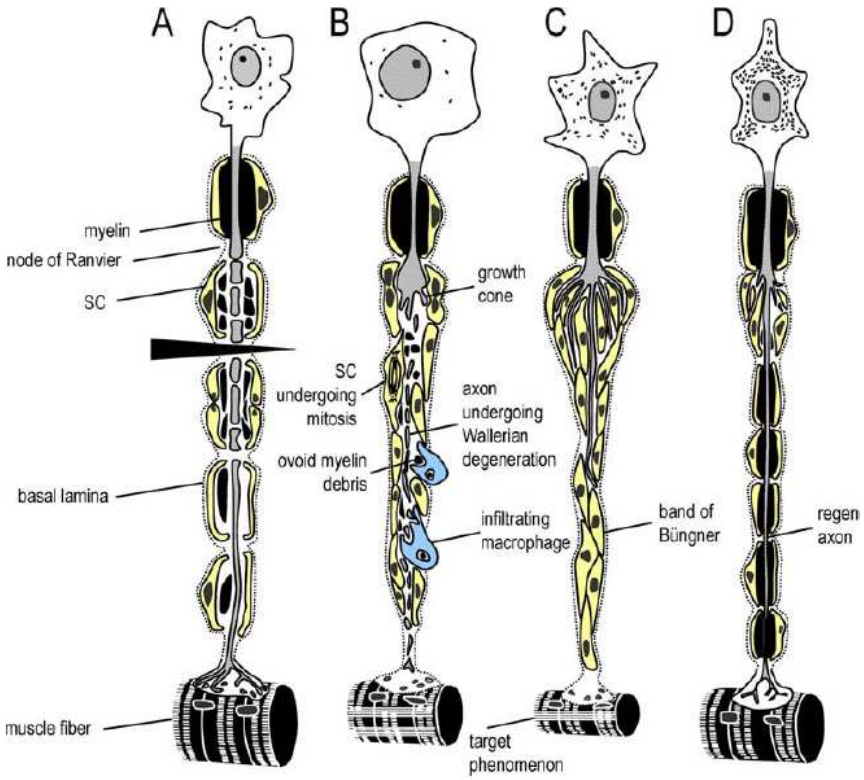

Figure 4.2 Morphological alterations following nerve injury: (A) Axotomy, (B) Chromatolysis in neurosoma accompanied by Wallerian degeneration of distal end of the axon and macrophage recruitment for phagocytosis of myelin debris. Growth cone formation at the proximal end of axon, (C) Schwann cell proliferation and alignment with endoneurial tube forming bands of Büngner which acts as substrate for proliferation, (D) Regeneration of axon and subsequent target innervation (Deumens et al. 2010)

4.2.2 Molecular response following peripheral neuron axotomy

An alteration of the gene expression for protein synthesis takes place in neuron cell body to stimulate increase in the synthesis of cytoskeletal components actin, tubulin and decrease in neurotransmitter transport functions. Peripheral neuron injury initiates molecular response involving induction of transcription factors, adhesion molecules and growth-associated proteins

and cytoskeletal components directed towards axon regeneration (Liu et al. 2011, Makwana and Raivich 2005). Activating Transcription Factor ATF3, a marker for neuronal injury is induced in L4-L5 DRGs and promotes axon regeneration in vivo (Pearson et al. 2003). Transcription factor cJun assists with axonal regeneration, target reinnervation and functional recovery (Zhou et al. 2004, Makwana and Raivich 2005).

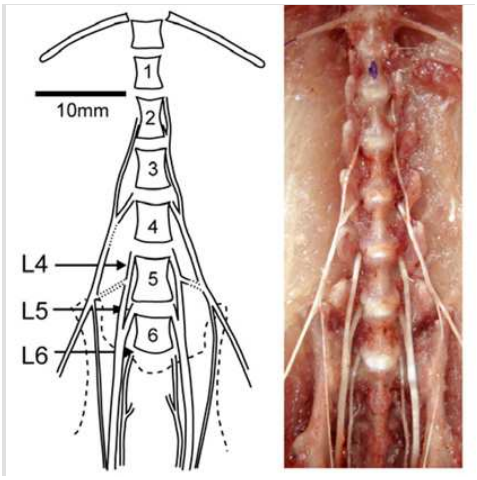

Figure 4.3 Illustration of L1-L6 Lumbar Dorsal Root: L4 and L5 DRGs are the main contributors of sciatic nerve (Rigaud et al 2008)

Following sciatic nerve injury, upregulation of transcription factors like cJun and ATF3 is seen in L4 and L5 DRGs since afferent axons of the rat sciatic nerve are supplied by the neurons of L3-L6 Dorsal Root Ganglions of which 99% of neuron somas are located in the L4 and L5 DRGs (Swett et al. 1991),

Biocompatible materials used for fabrication of microelectrodes such as Silicon and Platinum/Iridium have Young's modulus in the range of 135 GPa-165 GPa (Cheung 2010) whereas that of Brain tissue is ~3 kPa (Taylor and Miller 2004) and that of nerve tissue between 66 kPa and 266 kPa (Pfister et al. 2004). This difference in mechanical properties leads to neuronal injury at the interface when electrodes are implanted in tethered mode and electrodes move with respect to nerve tissue. ATF3 is upregulated in response to stress due to micromotion (Johansson et al. 2009). In our study, we compare transcription factor ATF3 levels in L5 DRGs of

control (empty conduit) and REMI implanted animals after 15, 30 and 60 days of implantation to evaluate the effect of REMI on nerve regeneration and whether the nerve is affected by micromotion. cJun levels were also assessed in control and REMI-implanted animals to compare nerve regeneration between the groups at 15, 30 and 60 days post-implantation.

4.3 Methods

4.3.1 Dorsal Root Ganglion extraction

Animals were sacrificed after 15, 30 and 60 days of surgery (n=6 for REMI implanted and n=4 for Control per time-point), by transcardial perfusion as described in section 3.2.1. The vertebral column was harvested, post-fixed overnight in 4% Paraformaldehyde (PFA) and then stored in 1X PBS. The ipsilateral and the contralateral L4 and L5 DRGs were extracted from the vertebral column.

4.3.2 Sample preparation and Cryosectioning

The tissues were kept overnight in 30% sucrose solution for cryoprotection and prepared for sectioning the next day. The DRGs were embedded by freezing the specimens in Optimal Cutting Temperature (OCT) freezing medium (Tissue Tek) by using Dry Ice and 100% alcohol. The blocks of embedded DRGs were stored at -80° C for cryosectioning. The blocks were sectioned at the thickness of 20 µm using Cryostat (Leica CM 1850) at -17 to -19° C. The sections were mounted on positive-charged slides.

4.3.3 Immunofluorescence staining

Table 4.1 Dilution factors of primary and secondary antibodies for cJun and ATF3 staining

Antigen	Blocking solution	Primary antibodies / Dilution	Secondary antibodies / Dilution
cJun	4% Donkey Normal Serum	Rabbit anti-cJun (Cell Signaling) / 1:300	DnαRb IgG Cy3 (Jackson Immunoresearch) / 1:300
ATF3	4% Goat Normal Serum	Rabbit anti-ATF3 (Santa-Cruz Biotechnology) / 1:100	GtαRb IgG Dylight 488 (Jackson Immunoresearch) / 1:300

The L4-L5 DRG sections were Immunostained for cJun and ATF3. The sections were washed three times in 1X PBS for 10 minutes. The slides were then incubated for one hour in blocking solution to block non-specific binding. The blocking solution was removed after an hour and the sections were incubated with primary antibodies overnight. Table 4.1 gives the details of the blocking solution and the concentrations of primary and secondary antibodies used for staining.

4.3.4 Image Analysis and Quantification

For cJun stained sections, the fluorescence imaging was carried out by using Carl Zeiss, Axiocam and for ATF3 stained sections, the images were taken by Zeiss LSM 510 Confocal microscope. Two images of distinct regions in L5 DRG were acquired at 20X objective per animal. cJun and ATF3 are localized in the nucleus of the DRG cells. For quantification, the number of cells expressing cJun or ATF3 was counted and the percentage with respect to the total number of cells was calculated.

4.3.5 Statistical Analysis

The percentages of cells expressing cJun in L5 DRGs between 15, 30 and 60-days after injury were compared. The statistical analysis was performed using unpaired student's t-test for unequal variances. p-values less than 0.05 were considered to be statistically significant (with the significance level $\alpha = 0.05$). The results were reported as mean ± standard deviation or mean ± standard error of the mean. The same procedure was carried out for ATF3 stained sections.

4.4 Results

Following a peripheral nerve injury, complex morphological and molecular changes are induced to promote regeneration of axons. Immediate Early genes (IEGs) cJun and ATF3 are upregulated rapidly after sciatic nerve transection. These IEGs have vital roles in molecular signaling to initiate the process of nerve regeneration. While ATF3 (Activating Transcription Factor-3) is a neuronal injury marker and assists in enhancing nerve regeneration, cJun

expression is required for efficient axonal regeneration and regulation of neuronal apoptosis. Representative images of ATF3 labeled ipsilateral L5 DRGs at 15, 30 and 60 days after surgery are shown in Figure 4.6. Figure 4.5 shows the graph which compares the percentage of ATF3 expressing DRG neurons between the three time-points. A significant decrease was seen in the percentage from 15-days to 60-days post-implantation. Furthermore, there was significant difference found between the percentages of ATF3 in REMI-implanted animals and control animals suggesting that REMI itself does not cause any nerve injury. Figure 4.8 shows cJun at 15, 30 and 60 days post-implantation for REMI implanted and for Control rats. Graph in Figure 4.7 demonstrates the trend of cJun and compares the REMI implanted animals with Control animals. A significant increase is seen from 15-days to 60-days post-implantation in REMI animals. No significant difference was found between the Control and REMI animals at each time-point. This suggests that the regeneration process in REMI implanted animals was not affected by the presence of electrodes in the sciatic nerve.

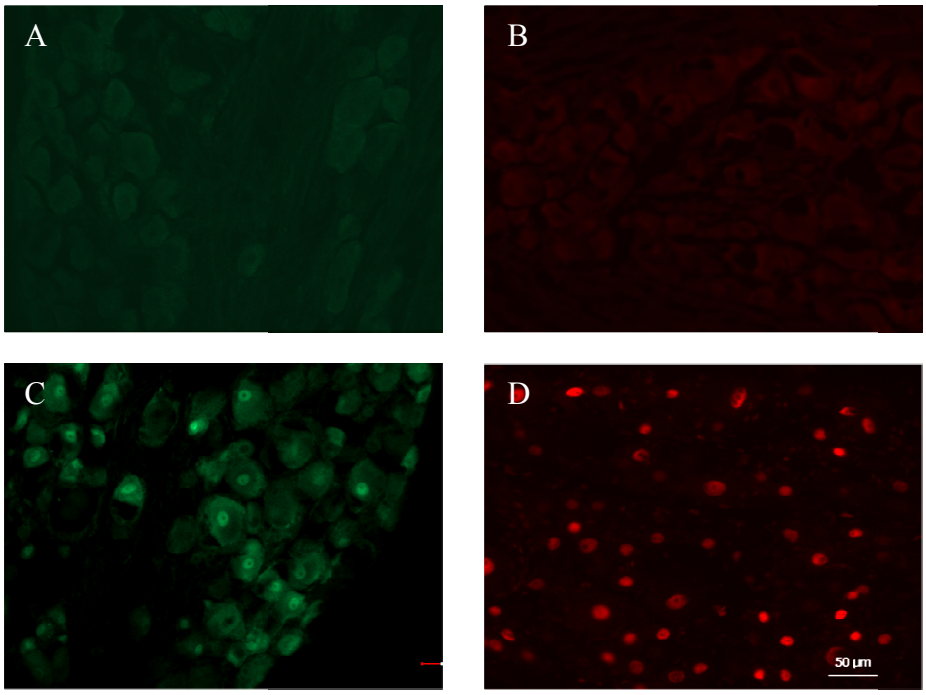

Figure 4.4 Representative images of L5 DRGs for: negative control (without Primary) (A) ATF3, (B) cJun, positive control (72 hours after sciatic nerve injury) (C) ATF3, (D) cJun

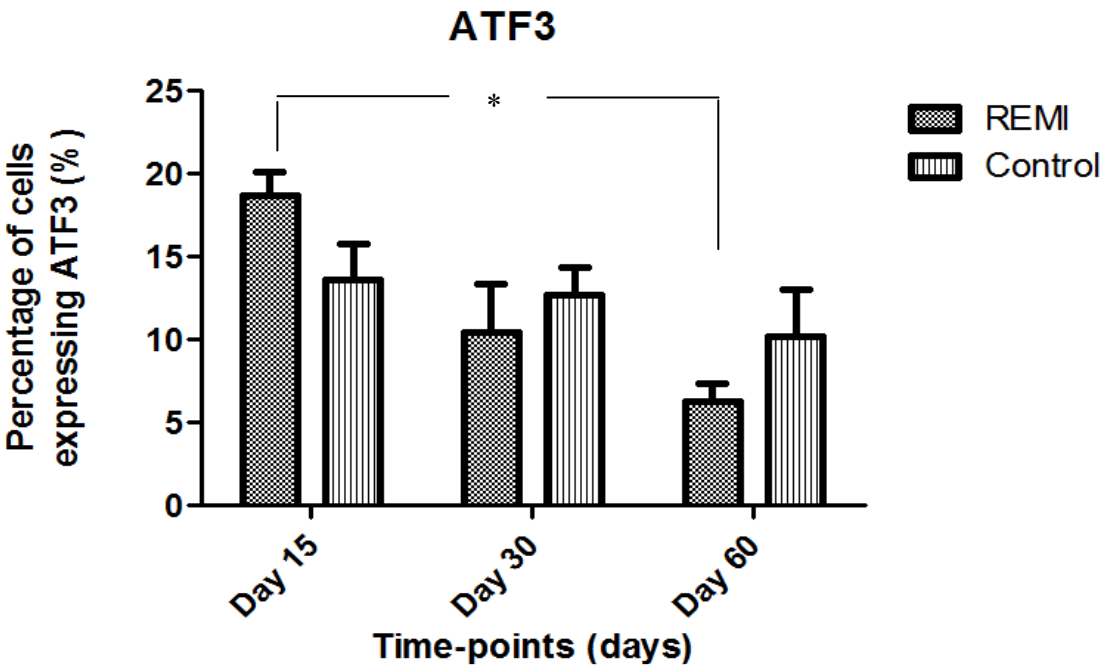

Figure 4.5 Comparison of percentage of L5 DRG cells expressing ATF3 after 15, 30 and 60 days of implantation (A) Control rats, (B) REMI implanted rats

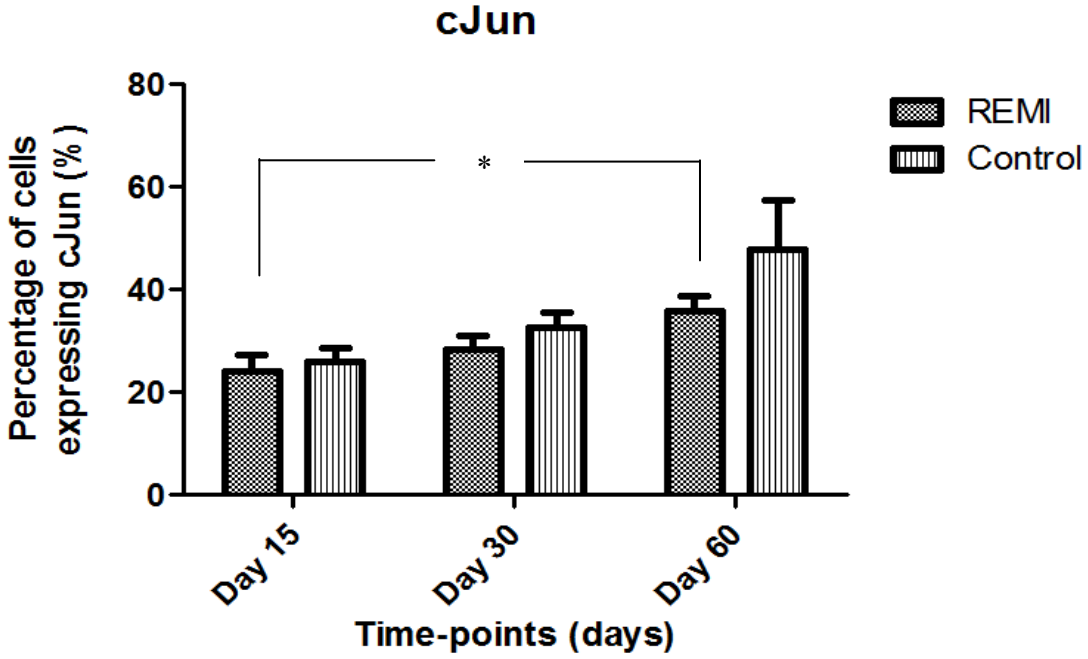

Figure 4.6 Comparison of percentage of L5 DRG cells expressing cJun at 15, 30 and 60 days post-implantation (A) Control rats, (B) REMI implanted rats

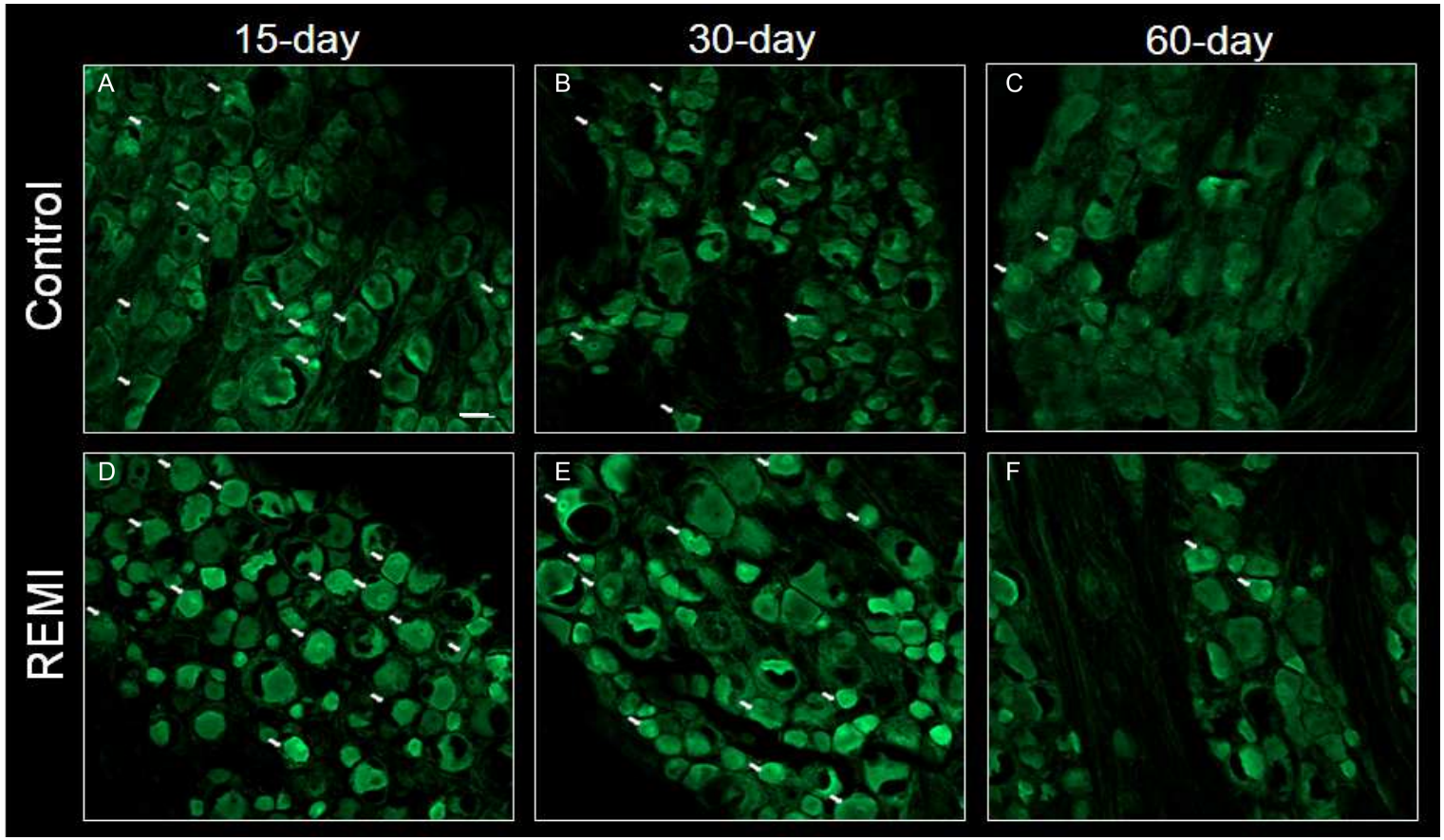

Figure 4.7 Representative images of ATF3 labeled L5 DRGs at 15 days, 30 days and 60 days after implantation comparing (A)-(C) Control rats and (D)-(F) REMI-implanted rats (Nuclei expressing ATF3 marked by white arrow) (Scale bar = 30 μm)

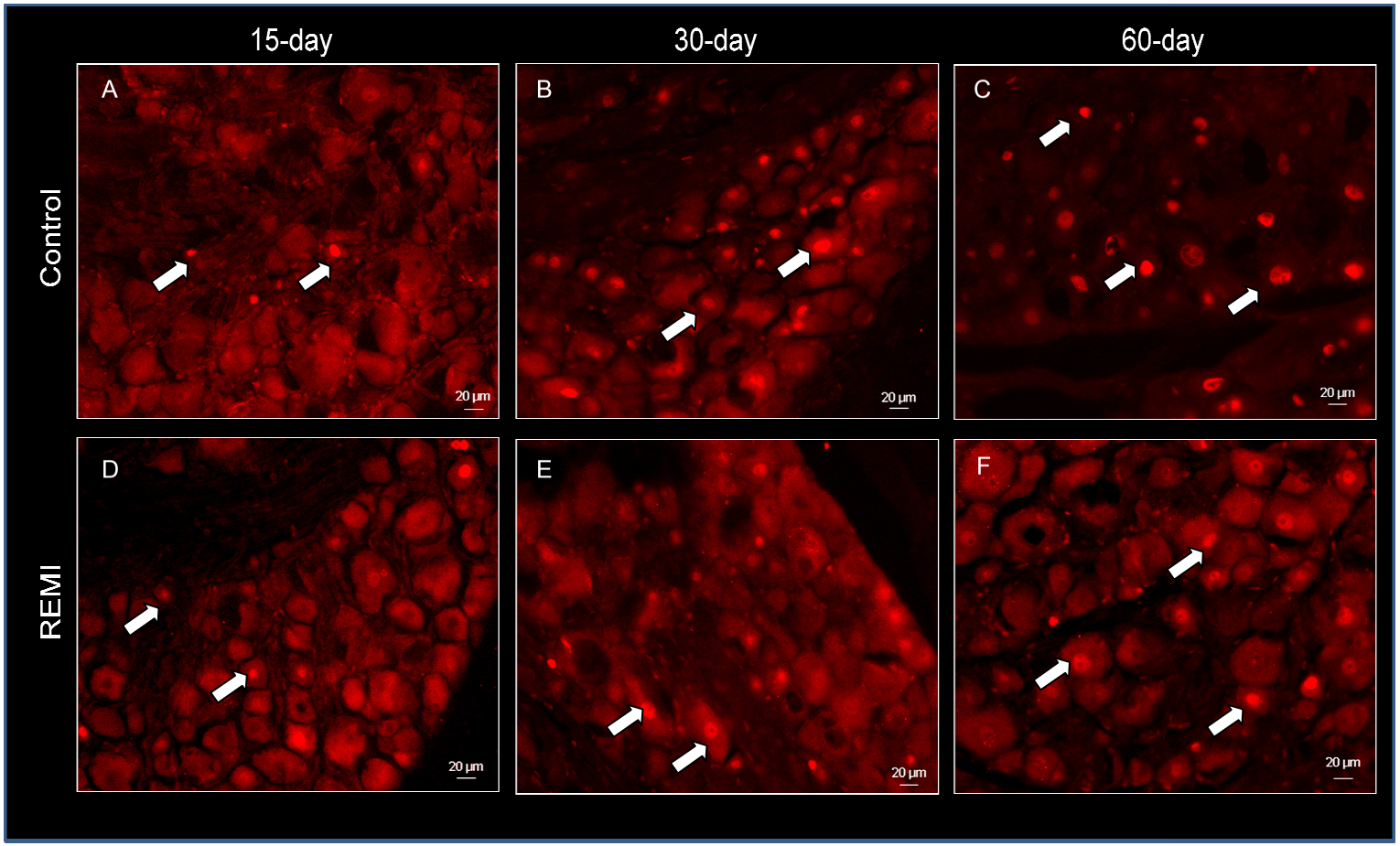

Figure 4.8 Representative images of cJun labeled L5 DRGs at 15 days, 30 days and 60 days post- implantation, comparing REMI-implanted rats (A)-(C) and Control rats (D)-(F). Expression of cJun is localized in nuclei (arrows)

4.5 Discussion

Activating Transcription Factor 3 (ATF3) is a direct marker for neuronal injury (Linda et al. 2011). ATF3 level is upregulated at day 15 post implantation in REMI and control animals. The significant decrease in ATF3 percentage from 15 days to 60 days after surgery and the difference between REMI and control animals being not significant suggest that the REMI implanted animals do not induce any neuronal injury due to micromotion. cJun levels increased significantly from 15-days to 60-days post-implantation. Moreover, no significant difference was seen between REMI implanted and control animals. However, it is observed that the levels of ATF3 are less at 60-days in REMI implanted animals than the control animals. A possible explanation of this difference could be that for REMI implanted animals, the FMA may provide some structural support for the nerve to regenerate and leads to decrease in ATF3 lower compared to control animals which have empty polyurethane conduits. This study eliminates micromotion as a source of nerve injury or of continual inflammatory response. The decay in the number of active sites is not related to foreign body tissue response or micromotion suggesting that factors other than the macrophage scar and micromotion may be causing the decline in the percentage of functional electrodes.

CHAPTER 5

CONCLUSION AND FUTURE WORK

Neural prosthetics interfacing robotic limb with the nervous system can assist amputees in controlling prosthetics with finer dexterity and allow manipulation of upper limb prosthesis having high degrees of freedom, thus can closely mimic natural limb. However, these neuroprosthetics are limited by their lack of reliability and are not feasible for long-term clinical use. Implantation of electrodes in central nervous system leads to decline in number of functional electrodes due to astrocyte glial scar formation at the site of implantation (Polikov et al. 2005, Rousche and Normann 2003). However, the cause of reduction of active sites in peripheral interfaces has not been established.

This study evaluated the role of inflammatory response in the decrease of number of active recording sites. We also investigated potential damage to the regenerating neurons due to micromotion. Electrophysiological results showed a reduction in percentage of active sites from 14 days to 42 days post-implantation. Further, the histological results assessing the foreign body-tissue response illustrated reduction in the macrophage scar at the implant-tissue interface from 15 days to 60 days after implantation. It is evident from these results that even in the presence of macrophage scar the implanted electrodes were capable of recording neural activity at 14 days, with maximum amplitude recorded on day 21. The macrophage scar does not compact after 60 days of implantation suggesting that factors other than the inflammatory response are causing the decay in the recorded neural activity.

The decay of quality of the recorded neural signal can be a result of neuronal injury due to micromotion. When implant moves with respect to the tissue, micromotion can contribute to injury of neurons and continual inflammatory response at the implantation site. Such tethered implants lead to reduction in neurons at the interface, thereby increasing the distance between

electrode tips and regenerating neurons. From the immunofluorescence results, ATF3 - a neuronal injury marker expressed in L4-L5 DRGs ipsilateral to the transected sciatic nerve, was observed to decrease significantly from day 15 to day 60 post-implantation in REMI-implanted animals. There was no significant difference between the REMI implanted animals and the control (empty conduits) animals. ATF3 results in conjunction with cJun results suggest that micromotion can be eliminated as a contributing factor for neuron injury or persistent foreign body-tissue response.

Seifert et al. (2011) reported neural activity recorded at 15 days after REMI implantation despite immature myelination. The early neural activity can be recorded despite the presence of macrophage scar at the electrode tip at day 15 post-implantation. By 60 days after the surgery, the macrophage scar area reduces significantly compared to that at 15 days. Though the inflammatory response appears to subside, a reduction in number of active electrodes is observed. In the process of normal regeneration of neurons, the axons myelinate and myelin layers envelope the axon forming an insulating sheath around the axon. Myelination maturation seems to correlate with the decrease in the number of functional electrodes. Whether myelination plays a role in the decay in the signal quality recorded needs to be further investigated. Elucidating the cause of failure of peripheral electrodes can facilitate enhancing the neural interfaces for chronic implantation, thus make available bionic limb which can better imitate natural limb functions and be clinically viable.

REFERENCES

Andersen RA, Musallam S and Pesaran B. Selecting the signals for a brain–machine interface. *Current Opinion in Neurobiology* 14(6): 720-726, 2004.

Badia J, Boretius T, Andreu D, Azevedo-Coste C, Stieglitz T and Navarro X. Comparative analysis of transverse intrafascicular multichannel, longitudinal intrafascicular and multipolar cuff electrodes for the selective stimulation of nerve fascicles. *Journal of neural engineering* 8: 1-13, 2011.

Behrend C, Reizner W, Marchessault JA and Hammert WC. Update on Advances in Upper Extremity Prosthetics. *The Journal of Hand Surgery* 36(10): 1711-1717, 2011.

Billock J. Upper Limb Prosthetic Terminal Devices: Hands Versus Hooks. *Clinical Prosthetics and Orthotics* 10(2): 57-65, 1986.

Biran R, Martin D, Tresco P. The brain tissue response to implanted silicon microelectrode arrays is increased when the device is tethered to the skull. *Experimental Neurology* 195(1):115-126, 2005.

Branner A, Stein RB and Normann RA. Selective Stimulation of Cat Sciatic Nerve Using an Array of Varying-Length Microelectrodes. *Journal of Neurophysiology* 85: 1585-1594, 2001.

Branner A, Stein RB, Fernandez E, Aoyagi Y and Normann RA. Long-Term Stimulation and Recording With a Penetrating Microelectrode Array in Cat Sciatic Nerve. *IEEE TRANSACTIONS ON BIOMEDICAL ENGINEERING* 51(1): 146-157, 2004.

Chapin JK, Moxon KA, Markowitz RS and Nicolelis MAL. Real-time control of a robot arm using simultaneously recorded neurons in the motor cortex. *Nature Neuroscience* 2(7): 664-670, 1999.

Chen ZL, Yu WM and Strickland S. Peripheral Regeneration. *Annual Review of Neuroscience* 30: 209-233, 2007.

Cheung K. Thin-Film Microelectrode Arrays for Biomedical Applications. *Implantable Neural Prostheses 2: Biological and Medical Physics, Biomedical Engineering* 157-190, 2010.

Cho S, Lu H, Cauller L, Romero-Ortega M, Lee J, Hughes G. Biocompatible SU-8-Based Microprobes for Recording Neural Spike Signals From Regenerated Peripheral Nerve Fibers. IEEE Sensors Journal 8(11):1830-1836, 2004.

Chung MS. Congenital Differences of the Upper Extremity: Classification and Treatment Principles. *Clinics in Orthopedic Surgery* 3: 172-177, 2011.

Cui X, Wiler J, Dzaman M, Altschuler RA and Martin DC. In vivo studies of polypyrrole/peptide coated neural probes. *Biomaterials* 24(5): 777-787, 2003.

Darnall BD, Ephraim P, Wegener ST, Dillingham T, Pezzin L, Rossbach P and MacKenzie EJ. Depressive Symptoms and Mental Health Service Utilization among Persons with Limb Loss: Results of a National Survey. *Archives of Physical Medicine and Rehabilitation* 86: 650-658, 2005.

Deumens R, Bozkurt A, Meek MF, Marcus M, Joosten E, Weis J, and Brook GA. Repairing injured peripheral nerves: Bridging the gap. Progress in Neurobiology 92: 245-276, 2010.

Dhillon GC and Horch KW. Direct Neural Sensory Feedback and Control of a Prosthetic Arm. *IEEE Transactions on Neural Systems and Rehabilitation Engineering* 13(4): 468-472, 2005.

Dillingham TR, Pezzin LE and MacKenzie EJ. Incidence, Acute Care Length of Stay, and Discharge to Rehabilitation of Traumatic Amputee Patients: An Epidemiologic Study. *Archives of Physical Medicine and Rehabilitation* 79(3): 279-287, 1998.

Dillingham TR, Pezzin LE and Mackenzie EJ. Limb Amputation and Limb Deficiency: Epidemiology and Recent Trends in the United States. *Southern Medical Journal* 95(8): 875-883, 2002.

Fitzgerald RH, Mills JL, Joseph W and Armstrong DG. The Diabetic Rapid Response Acute Foot Team: 7 Essential Skills for Targeted Limb Salvage. *Eplasty* 9, 2009.

Garcia LA. Epidemiology and Pathophysiology of Lower Extremity Peripheral Arterial Disease. *Journal of Endovascular Therapy* 13(II): 3-9, 2006.

Garde K, Keefer E, Botterman B, Galvan P, Romero MI. Early Interfaced Neural Activity from Chronic Amputated Nerves. *Frontiers in Neuroengineering* 2(5), 2009.

Hassler C, Boretius T and Stieglitz T. Polymers for neural implants. *Journal of Polymer Science Part B: Polymer Physics* 49(1): 18-33, 2011.

Hoffer J. Techniques to Study Spinal-Cord, Peripheral Nerve, and Muscle Activity in Freely Moving Animals. *Neurophysiological Techniques-Neuromethods* 15:65-145, 1991.

Jacobsen SC, Knutti DF, Johnson RT and Sears HH. Development of the Utah Artificial Arm. *IEEE Transactions on Biomedical Engineering BME*-29(4): 249-269, 1982.

Johansson F, Wallman L, Danielsen N, Schouenborg J and Kanje M. Porous silicon as a potential electrode material in a nerve repair setting: Tissue reactions. *Acta Biomaterialia* **5**: 2230–2237, 2009.

Kim S, Simeral J, Hochberg L, Donoghue J, Black M. Neural control of computer cursor velocity by decoding motor cortical spiking activity in humans with tetraplegia. *Journal of Neural Engineering* 5(4): 455-476, 2008.

Kirk KL, Jones EM, Potter BK, Osborn PM and Ficke JR. Partial Foot Amputations in the Combat Wounded. *Journal of Surgical Orthopaedic Advances* 20(1): 19-22, 2011.

Klinge PM, Vafa MA, Brinker T, Brandis A, Walter GF, Stieglitz T, Samii M and Wewetzer K. Immunohistochemical characterization of axonal sprouting and reactive tissue changes after long-term implantation of a polyimide sieve electrode to the transected adult rat sciatic nerve. *Biomaterials* 22(17): 2333-2343, 2001.

Kuchenbecker KJ, Gurari N and Okamura AM. Effects of Visual and Proprioceptive Motion Feedback on Human Control of Targeted Movement. *IEEE*: 513-524, 2007.

Kuiken T. Targeted reinnervation for improved prosthetic function. *Physical Medicine and Rehabilitation clinics of North America* 17(1): 1-13, 2006.

Kuiken TA, Miller LA, Lipschutz RD, Lock BA, Stubblefield K, Marasco PD, Zhou P and Dumanian GA. Targeted reinnervation for enhanced prosthetic arm function in a woman with a proximal amputation: a case study. *The Lancet* 369(9559): 371-380, 2007.

Kuiken TA, Marasco PD, Lock BA, Harden RN and Dewald J. Redirection of cutaneous sensation from the hand to the chest skin of human amputees with targeted reinnervation. *Proceedings of the National Academy of Sciences* 104(50): 20061–20066, 2007.

Lago N, Yoshida K, Koch K and Navarro X. Assessment of Biocompatibility of Chronically Implanted Polyimide and Platinum Intrafascicular Electrodes. IEEE Transactions on Biomedical Engineering 54(2): 281-290, 2007.

Lebedev MA and Nicolelis MAL. Brain–machine interfaces: past, present and future. *Trends in Neurosciences* 29(9): 536-546, 2006.

Lefurge T, Goodall E, Horch K, Stensaas L and Schoenberg A. Chronically Implanted Intrafascicular Recording Electrodes. *Annals of Biomedical Engineering* 19: 197-207, 1991.

Light CM, Chappell PH, Hudginsz B and Engelhartz K. Intelligent multifunction myoelectric control of hand prostheses. *Journal of Medical Engineering & Technology* 26(4): 139-146, 2002.

Lindå H, Sköld MK and Ochsmann T. Activating transcription factor 3, a useful marker for regenerative response after nerve root injury. *Frontiers in Neurology* 2(30), 2011.

Liu K, Tedeschi A, Park KK and He Z. Neuronal Intrinsic Mechanisms of Axon Regeneration. *Annual Review of Neuroscience* 34:131-152, 2011.

Logothetis N. The neural basis of the blood-oxygen-level-dependent functional magnetic resonance imaging signal. *Philosophical Transactions of the Royal Society* 357(1424):1003-1037, 2002.

Lotfi P, Garde K, Chouhan AK, Bengali E and Romero-Ortega MI. Modality-specific axonal regeneration: toward selective regenerative neural interfaces. *Frontiers in Neuroengineering* 4(11), 2011.

Malmstrom J, McNaughton T, Kenneth W. Recording Properties and Biocompatibility of Chronically Implanted Polymer-based Intrafascicular Electrodes. *Annals of Biomedical Engineering* 26(6):1055-1064, 1998.

Makwana M and Raivich G. Molecular mechanisms in successful peripheral regeneration. *FEBS Journal* 272: 2628–2638, 2005.

Mattia M, Ferraina S and Giudice PD. Dissociated multi-unit activity and local field potentials: A theory inspired analysis of a motor decision task. *NeuroImage* 52: 812-823, 2010.

Mautner GC, Mautner SL and Roberts WC. Amounts of coronary arterial narrowing by atherosclerotic plaque at necropsy in patients with lower extremity amputation. *The American Journal of Cardiology* 70(13): 1147-1151, 1992.

Maynard EM, Nordhausen CT and Normann RA. The Utah Intracortical Electrode Array: A recording structure for potential brain-computer interfaces. *Electroencephalography and Clinical Neurophysiology* 102(3): 228-239, 1997.

McConnell GC, Schneider TM, Owens DJ and Bellamkonda RV. Extraction Force and Cortical Tissue Reaction of Silicon Microelectrode Arrays Implanted in the Rat Brain. *IEEE Transactions on Biomedical Engineering* 54(6): 1097–1107, 2007.

Mensinger AF, A. D., Buchko CJ, Johnson MA, Martin DC, Tresco PA, Silver RB and Highstein SM. Chronic Recording of Regenerating VIIIth Nerve Axons With a Sieve Electrode. *Journal of Neurophysiology* 83(1): 611-615, 2000.

Micera S, Carpaneto J and Raspopovic S. Control of Hand Prostheses Using Peripheral Information. *IEEE Reviews in Biomedical Engineering* 3: 48-68, 2010.

Millstein Sg, Heger H and Hunter Ga. Prosthetic use in adult upper limb amputees: a comparison of the body powered and electrically powered prostheses. *Prosthetics and Orthotics International* 10: 27-34, 1986.

Mussa-Ivaldi F and Miller L. Brain–machine interfaces: computational demands and clinical needs meet basic neuroscience. *Trends in Neuroscience* 26(6): 329-334, 2003.

Navarro X, Krueger TB, Lago N, Micera S, Stieglitz T and Dario P. A critical review of interfaces with the peripheral nervous system for the control of neuroprostheses and hybrid bionic systems. *Journal of the Peripheral Nervous System* 10(3): 229–258, 2005.

Nicolelis M, Dimitrov D, Carmena J, Crist R, Lehew G, Kralik J, Wise S. Chronic, multisite, multielectrode recordings in macaque monkeys. *Proceedings of the National Academy of Sciences* 100(19):11041-11046, 2003.

Pearson A, Gray CW, Pearson JF, Greenwood JM, During MJ, Dragunow M. ATF3 enhances c-Jun-mediated neurite sprouting. *Molecular Brain Research* **120**(1): 38-45, 2003.

Pettingill LN, Richardson RT, Wise AK, O'Leary SJ and Shepherd RK. Neurotrophic Factors and Neural Prostheses: Potential Clinical Applications Based Upon Findings in the Auditory System. *IEEE Transactions on Biomedical Engineering* 54(6): 1138-1148, 2007.

Pezzin LE, Dillingham TR, MacKenzie EJ, Ephraim P and Rossbach P. Use and satisfaction with prosthetic limb devices and related services. *Archives of Physical Medicine and Rehabilitation* 85(5): 723-729, 2004.

Pfister LA, Christen T, Merkle HP, Papaloïzos M and Gander B. Novel Biodegradable Nerve Conduits for Peripheral Nerve Regeneration. *European Cells and Materials* 7(2): 16-17, 2004.

Phillips J, Smit X, Zoysa N, Afoke A, Brown R. The brain tissue response to implanted silicon microelectrode arrays is increased when the device is tethered to the skull. *Journal of Physiology* 557(3):879-887, 2004.

Polikov VS, Tresco PA and Reichert WM. Response of brain tissue to chronically implanted neural electrodes. *Journal of Neuroscience Methods* 148: 1-18, 2005.

Polikov V, Block M, Fellous J, Hong J, Reichert W. In vitro model of glial scarring around neuroelectrodes chronically implanted in the CNS. *Biomaterials* 27(31):5368-5376, 2006.

Quiroga RQ, Nadasdy Z and Ben-Shaul Y. Unsupervised Spike Detection and Sorting with Wavelets and Superparamagnetic Clustering. *Neural Computation* 16: 1661–1687, 2004.

Rees G, Kreiman G and Koch C. Neural Correlates of Consciousness in Humans. *Nature Reviews Neuroscience* 3: 261-270, 2002.

Reiber GE, Vileikyte L, Boyko EJ, Aguila MD, Smith DG, Lavery LA and Boulton AJM. Causal Pathways for Incident Lower- Extremity Ulcers in Patients with Diabetes from Two Settings. *Diabetes Care* 22(1): 157-162, 1999.

Rennaker RL, Streeta S, Ruylea AL and Sloan AM. A comparison of chronic multi-channel cortical implantation techniques: manual versus mechanical insertion. *Journal of Neuroscience Methods* 142(2): 169-176, 2005.

Rigaud M, Gemes G, Barabas ME, Chernoff DI, Abram SE, Stucky CL and Hogan QH. Species and strain differences in rodent sciatic nerve anatomy: implications for studies of neuropathic pain. *Pain* 136(1-2): 188-201, 2008.

Rothschild RM. Neuroengineering Tools/Applications for Bidirectional Interfaces, Brain–Computer Interfaces, and Neuroprosthetic Implants – A Review of Recent Progress. *Frontiers in Neuroengineering* 3(112), 2010.

Rousche P and Normann R. Chronic recording capability of the Utah Intracortical Electrode Array in cat sensory cortex. *Journal of Neuroscience methods* 82(1):1-15, 1998.

Schmidt EM, Mcintosh JS and Bak MJ. Long-term implants of Parylene-C coated microelectrodes. *Medical and Biological Engineering and Computing* 26(1): 96-101, 1988.

Schulman JH. Brain Control and Sensing of Artificial Limbs. *Implantable Neural Prostheses 1 - Biological and Medical Physics, Biomedical Engineering*: 275-291, 2009.

Schwartz AB, Cui T, Weber DJ and Moran DW. Brain-Controlled Interfaces: Movement Restoration with Neural Prosthetics. *Neuron* 52(1): 205-220, 2006.

Seifert JL, Desai V, Watson RC, Musa T, Kim YT, Keefer EW, Romero MI. Increasing Spike Activity Recorded from Regenerative Peripheral Nerve Interfaces in the First Two Weeks Post-Implantation Despite Immature Myelination. IEEE, 2011.

Serruya MD, Hatsopoulos NG, Paninski L, Fellows MR and Donoghue JP. Brain-machine interface: Instant neural control of a movement signal. *Nature* 416: 141-142, 2002.

Soechting JF and Flanders M. Flexibility and Repeatability of Finger Movements during Typing: Analysis of Multiple Degrees of Freedom. *Journal of Computational Neuroscience* 4: 29–46, 1997.

Stubblefield KA, Miller LA, Lipschutz RD and Kuiken TA. Occupational therapy protocol for amputees with targeted muscle reinnervation. *Journal of Rehabilitation Research and Development* 46(4): 481-488, 2009.

Swett JE, Torigoe Y, Elie VR, Bourassa CM and Miller PG. Sensory neurons of the rat sciatic nerve. *Experimental Neurology* 114(1): 82-103, 1991.

Taylor Z and Miller K. Reassessment of brain elasticity for analysis of biomechanisms of hydrocephalus. *Journal of Biomechanics* 37(8): 1263-1269, 2004.

Thelin J, Jorntell H, Psouni E, Garwicz M, Schouenborg J, Danielsen N, Linsmeier C. Implant Size and Fixation Mode Strongly Influence Tissue Reactions in the CNS. *PLoS One* 6(1), 2011.

Thurston AJ. Pare´ and prosthetics: the early history of artificial limbs. *Anz Journal of Surgery* 77(12): 1114-1119, 2007.

Warwick K, Gasson M, Hutt B,Goodhew I, Kyberd P, Andrews B, Teddy P, Shad A. The Application of Implant Technology for Cybernetic Systems. *Archives of Neurology* 60(10):1369-1373, 2003.

Zhou FQ, Walzer MA and Snider WD. Turning on the Machine: Genetic Control of Axon Regeneration by c-Jun. *Neuron* 43: 1-4, 2004.

Zhong Y and Bellamkonda RV. Controlled release of anti-inflammatory agent α-MSH from neural implants. *Journal of Controlled Release* 106(3): 309-318, 2005.

Ziegler-Graham K, MacKenzie EJ, Ephraim PL, Travison TG and Brookmeyer R. Estimating the prevalence of limb loss in the United States: 2005 to 2050. *Archives of Physical Medicine and Rehabilitation* 89(3): 422-429, 2008.

BIOGRAPHICAL INFORMATION

Nivedita Khobragade received her Bachelor's degree in Electronics Engineering from one of the most distinguished colleges in India, Veermata Jijabai Technological Institute (VJTI), Mumbai, India, in June 2007. She then worked as a Software engineer in HSBC Global Technologies Limited, Pune, India for two years starting from July 2007. She began her Graduate studies in Bioengineering at University of Texas at Arlington in Fall 2009. Driven by her penchant towards neuroengineering, she joined the laboratory of Dr. Mario I. Romero-Ortega and started working as a Graduate Research Assistant in Regenerative Neurobiology Lab from Jan. 2011.